The Astronomical Journal, 126:2209–2229, 2003 November

A LARGE, UNIFORM SAMPLE OF X-RAY–EMITTING AGNs: SELECTION APPROACH AND AN INITIAL CATALOG FROM THE *ROSAT* ALL-SKY AND SLOAN DIGITAL SKY SURVEYS

Scott F. Anderson,[1] Wolfgang Voges,[2] Bruce Margon,[3] Joachim Trümper,[2] Marcel A. Agüeros,[1] Thomas Boller,[2] Matthew J. Collinge,[4] L. Homer,[1] Gregory Stinson,[1] Michael A. Strauss,[4] James Annis,[5] Percy Gómez,[6] Patrick B. Hall,[4,7] Robert C. Nichol,[6] Gordon T. Richards,[4] Donald P. Schneider,[8] Daniel E. Vanden Berk,[9] Xiaohui Fan,[10] Željko Ivezić,[4] Jeffrey A. Munn,[11] Heidi Jo Newberg,[12] Michael W. Richmond,[13] David H. Weinberg,[14] Brian Yanny,[5] Neta A. Bahcall,[4] J. Brinkmann,[15] Masataka Fukugita,[16] and Donald G. York[17]

Received 2003 May 5; accepted 2003 August 12

ABSTRACT

Many open questions in X-ray astronomy are limited by the relatively small number of objects in uniform optically identified and observed samples, especially when rare subclasses are considered or when subsets are isolated to search for evolution or correlations between wavebands. We describe the initial results of a new program aimed to ultimately yield $\sim 10^4$ fully characterized X-ray source identifications—a sample about an order of magnitude larger than earlier efforts. The technique is detailed and employs X-ray data from the *ROSAT* All-Sky Survey (RASS) and optical imaging and spectroscopic follow-up from the Sloan Digital Sky Survey (SDSS); these two surveys prove to be serendipitously very well matched in sensitivity. As part of the SDSS software pipelines, optical objects in the SDSS photometric catalogs are automatically positionally cross-correlated with RASS X-ray sources. Then priorities for follow-on SDSS optical spectra of candidate counterparts are automatically assigned using an algorithm based on the known ratios of f_x/f_{opt} for various classes of X-ray emitters at typical RASS fluxes of $\sim 10^{-13}$ ergs cm^{-2} s^{-1}. SDSS photometric parameters for optical morphology, magnitude, and colors, plus FIRST radio information, serve as proxies for object class. Initial application of this approach to RASS/SDSS data from 1400 deg^2 of sky provides a catalog of more than 1200 spectroscopically confirmed quasars and other AGNs that are probable RASS identifications. Most of these are new identifications, and only a few percent of the AGN counterparts are likely to be random superpositions. The magnitude and redshift ranges of the counterparts are very broad, extending over $15 < m < 21$ and $0.03 < z < 3.6$, respectively. Although most identifications are quasars and Seyfert 1 galaxies, a variety of other AGN subclasses are also sampled. Substantial numbers of rare AGN types are found, including more than 130 narrow-line Seyfert 1 galaxies and 45 BL Lac candidates. These early results already provide a very sizable set of source identifications, demonstrate the utility of the sample in multiwaveband investigations, and show the capability of the joint RASS/SDSS approach to efficiently proceed toward the largest homogeneously selected/observed sample of X-ray–emitting quasars and other kinds of AGNs.

Key words: catalogs — quasars: general — surveys — X-rays

On-line material: machine-readable tables

1. INTRODUCTION

Although extrasolar X-ray sources were first observed four decades ago (Giacconi et al. 1962), the first all-sky *imaging* X-ray survey has only recently been achieved. The *ROSAT* All-Sky Survey (RASS; Voges et al. 1999, 2000) covers the entire celestial sphere in the 0.1–2.4 keV range with the Position Sensitive Proportional Counter (PSPC; Pfeffermann et al. 1988) to a typical limiting sensitivity of $\sim 10^{-13}$ ergs cm^{-2} s^{-1}, although because of the scanning protocol, the

[1] Department of Astronomy, University of Washington, Box 351580, Seattle, WA 98195; anderson@astro.washington.edu.
[2] Max-Planck-Institut für extraterrestrische Physik, Geissenbachstrasse 1, D-85741 Garching, Germany; wvoges@mpe.mpg.de.
[3] Space Science Telescope Institute, 3700 San Martin Drive, Baltimore, MD 21218; margon@stsci.edu.
[4] Princeton University Observatory, Peyton Hall, Princeton, NJ 08544.
[5] Fermi National Accelerator Laboratory, P.O. Box 500, Batavia, IL 60510.
[6] Department of Physics, Carnegie Mellon University, 5000 Forbes Avenue, Pittsburgh, PA 15232.
[7] Departamento de Astronomía y Astrofísica, Facultad de Física, Pontificia Universidad Católica de Chile, Casilla 306, Santiago 22, Chile.
[8] Department of Astronomy and Astrophysics, Pennsylvania State University, University Park, PA 16802.
[9] Department of Physics and Astronomy, University of Pittsburgh, Pittsburgh, PA 15260.
[10] Steward Observatory, University of Arizona, 933 North Cherry Avenue, Tucson, AZ 85732.
[11] US Naval Observatory, Flagstaff Station, P.O. Box 1149, Flagstaff, AZ 86002.
[12] Department of Physics, Applied Physics, and Astronomy, Rensselaer Polytechnic Institute, 110 Eighth Street, Troy, NY 12180.
[13] Department of Physics, Rochester Institute of Technology, 85 Lomb Memorial Drive, Rochester, NY 14623-5603.
[14] Department of Astronomy, Ohio State University, 140 West 18th Avenue, Columbus, OH 43210.
[15] Apache Point Observatory, P.O. Box 59, Sunspot, NM 88349.
[16] Institute for Cosmic Ray Research, University of Tokyo, Midori, Tanashi, Tokyo 188-8588, Japan.
[17] Astronomy and Astrophysics Center, University of Chicago, 5640 South Ellis Avenue, Chicago, IL 60637.

exposure times and thus sensitivity limits vary markedly from the ecliptic pole to the equator. Depending on the level of statistical significance discussed, 10^4–10^5 X-ray sources are contained in the RASS Bright and Faint Source Catalogs, with more than 124,000 sources in the catalog versions considered here. Positional accuracies derivable for the sources vary with count rate, but moderately well-exposed sources typically have a positional uncertainty of $\sim 10''$–$30''$. Many important inferences can and have been made from RASS data based directly on the X-ray observations alone, with minimal need for new correlative observations at other wavelengths. For example, the RASS point source catalogs provide an exceptional measure of a portion of the X-ray $\log N/\log S$ diagram (e.g., Voges et al. 1999).

However, the scale of the effort involved in identifying a large fraction of the abundant RASS sources, especially those in the Faint Source Catalog, poses an unusual analysis problem. From *ROSAT* and also previous generations of X-ray observatories, especially the extensive observations of the *Einstein Observatory* (e.g., Gioia et al. 1984), such X-ray source counterparts are known to include a highly heterogeneous mix of objects, ranging from nearby M dwarfs to distant quasars. In many cases, the X-ray data taken alone cannot unambiguously determine whether an X-ray source is Galactic or extragalactic, much less finer distinctions about its nature. It has thus long been realized that identification of optical counterparts is an essential companion study to large X-ray surveys.

The most complete optical identification effort attempted on *Einstein* X-ray data was that of the Extended Medium Sensitivity Survey (EMSS; e.g., Stocke et al. 1991). The comparison with RASS is not inappropriate, since although *Einstein* surveyed less than 10% of the celestial sphere, the flux levels and positional accuracy of source determinations from the *Einstein* Imaging Proportional Counter detector were not greatly dissimilar to those from the *ROSAT* PSPC (though, for example, the latter provides better positional information). Optical identification of sources in the EMSS have been made in an exceptionally ambitious, decade-long program (e.g., Stocke et al. 1991 and references therein), with confirming optical spectra taken one at a time, using a heterogeneous collection of telescopes and detectors, the only plausible facilities available at that time. The EMSS yielded an impressive $\sim$800 optical counterparts, including normal stellar coronae, pre–main-sequence stars, interacting binaries, supernova remnants, nearby galaxies, clusters of galaxies, and especially active galactic nuclei (AGNs) of a broad range of luminosities. Quasars/AGNs are the predominant class in the EMSS, accounting for more than 400 of the *Einstein* identifications.

In a similar effort devoted to *ROSAT* data, there have been successful optical identification programs conducted, or still in progress, on bright subsets of the RASS or complete subsets over small regions of sky, by a large collaboration (Fischer et al. 1998; Zickgraf et al. 1998; Schwope et al. 2000). The goal is again $\sim 10^3$ optical identifications. In addition, a remarkably resourceful effort using the Hamburg objective prism plates (Bade et al. 1998a; Zickgraf et al. 2003) has resulted in the tabulation of candidate identifications for a significant number of the brightest RASS sources. Typically AGNs are inferred as the correct identification if an object with $B < 18.5$ has a blue continuum color over the 2000 Å of plate coverage; often emission lines are not detectable. However, even for this brighter subset, accurate redshifts, magnitudes, optical continuum slopes and emission-line identifications, intensities, and equivalent widths are largely unavailable.

Although the $\sim 10^3$ total identifications from $\sim 10^3$ deg^2 of sky provided by the EMSS (and similar later *ROSAT* surveys) is an extremely respectable number, there remain scientific problems where the size of an identified *subclass* of X-ray emitters of interest is uncomfortably small. Notable examples include studies of the more rare subclasses of AGNs, such as narrow-line Seyfert 1's (NLSy1's) and BL Lac objects. For example, among the large sample of more than 400 AGNs from the EMSS, only about $\sim$40 BL Lac objects were found, and yet, even this small subsample suggested remarkable "negative evolution" (e.g., Morris et al. 1991) that demands further study. If such rare subclasses of AGNs evolve in their properties with redshift and/or exhibit complex dependencies of X-ray luminosity with optical and/or radio luminosity, as more typical quasars are known to do (e.g., Avni & Tananbaum 1986; Wilkes et al. 1994; Avni, Worrall, & Morgan 1995), then an already small subsample must be further subdivided into yet smaller bins for analysis, leaving literally a handful of objects per bin. Another less obvious example is that although modest- to high-redshift quasars are not usually thought of as "rare," X-ray selection at the *Einstein* and RASS flux levels strongly favors the discovery of nearby and low-luminosity AGNs; in fact, the entire EMSS sample of greater than 400 AGNs includes only a small handful of X-ray–emitting quasars with $z > 2$, thus limiting its utility for studies of the quasar X-ray luminosity function at moderate to high redshift.

In order to effectively build and expand on such earlier large-scale counterpart identification programs, any new effort (at comparable X-ray depth) must survey substantially in excess of the $\sim 10^3$ deg^2 covered by the EMSS and must ultimately provide a sample numbering substantially in excess of $\sim 10^3$ optical identifications, obtained in a uniform fashion. Moreover, if many more than 10^3 counterparts are to be newly found on a reasonable timescale, more efficient optical identification techniques than previously available must be used. The requisite large X-ray sample is now available via the RASS Bright and Faint Source Catalogs; the more efficient optical identification and analysis technique is provided by the Sloan Digital Sky Survey (SDSS, e.g., York et al. 2000; Stoughton et al. 2002; Abazajian et al. 2003).

In this paper we describe the initial results of a program that exploits the unique combined capabilities of the *ROSAT* and Sloan surveys to eventually obtain a sample of $\sim 10^4$ X-ray sources, which are not only optically identified, but which also have high quality and uniform data in the X-ray from RASS and in the optical (photometry and spectroscopy) from SDSS. Our emphasis in this initial paper is on high-confidence RASS/SDSS optical identifications of quasars and other AGNs. In § 2 we provide a brief description of relevant aspects of the SDSS data and the fortuitous match in sensitivity to the RASS. In § 3, we detail the technique used to select and confirm candidate counterparts from the SDSS data. In § 4, we present results from this RASS/SDSS program for 1400 deg^2 of sky, providing an initial catalog (optical photometry and spectroscopy, as well X-ray properties) of more than 1200 likely AGN identifications for RASS X-ray sources, including 45 BL Lac candidates. In § 5, we discuss a few additional AGN subcategories and objects of special interest, including NLSy1's. Section 6

provides an overview of the ensemble properties of the initial sample, especially as they pertain to the reliability of the identifications. Section 7 provides an illustrative example of optical/X-ray correlation studies that may be enabled by the sample. A very brief summary is provided in § 8.

2. THE EXCELLENT MATCH BETWEEN SDSS OPTICAL AND RASS X-RAY SURVEYS

The Sloan Digital Sky Survey (SDSS) is a multi-institutional project to create an optical digital imaging and spectroscopic data bank of a large portion of the celestial sphere, mainly in a region approaching $\sim 10^4$ deg^2 centered on the north Galactic polar cap. A recent overview of the project has been given by York et al. (2000), and a comprehensive technical description of the large subset of the software pipelines and data released earlier to the public is available in Stoughton et al. (2002). The optical data are obtained by a special purpose 2.5 m telescope, located at Apache Point Observatory, New Mexico, built and optimized solely for this project. It is equipped with a unique mosaic camera (Gunn et al. 1998) that operates in TDI (Time Delay and Integrate) mode that can image $\sim 10^2$ deg^2 in five colors in a single night, as well as a multifiber spectrograph that obtains the spectra of 640 objects within a 7 deg^2 field simultaneously. The resulting photometric atlas is in five specially chosen colors u, g, r, i, z (Fukugita et al. 1996; Hogg et al. 2001; Smith et al. 2002) from $\sim$3600 to 10,000 Å, covering the entire survey area to a limiting magnitude of $r \sim 22$–23, on 0.″4 pixels. This database is automatically analyzed to catalog the photometric and astrometric properties of several hundred million stars and galaxies, as well as a million quasars. The imaging database is used to autonomously and homogeneously select objects for the SDSS spectroscopic survey, which will ultimately include moderate resolution ($\lambda/\Delta\lambda \sim 1800$) spectrophotometry covering a broad (3800–9200 Å) wavelength regime for 10^6 galaxies, 10^5 quasars, and 10^5 unusual stars.

The RASS and SDSS are extremely well-matched to each other via a variety of fortunate coincidences. For example, the SDSS survey area is also the region of greatest RASS X-ray sensitivity, because it lies primarily at high ecliptic latitude (and thus long RASS exposure times) and also high Galactic latitude (and thus regions of low interstellar photoelectric opacity, an important effect in the soft *ROSAT* energy band).

Perhaps most important, the limiting X-ray flux of RASS is such that, given the known range of f_x/f_{opt} for most common classes of sources, both Galactic and extragalactic, even the optically faintest counterparts of typical RASS sources are accessible to both the SDSS photometric and spectroscopic surveys. For example, although there is considerable dispersion, the most X-ray luminous (relative to optical) normal stars, normal galaxies, quasars, and BL Lac objects are known to have log (f_x/f_{opt}) of about -1, -0.25, 1.0, and 1.5, respectively (e.g., Stocke et al. 1991). At the limiting RASS X-ray flux quoted above, this implies that even unusually faint optical counterparts in each of these classes will have magnitudes brighter than $m \sim 15$, 17, 20, and 21, respectively. Thus, the SDSS imaging survey will obtain highly accurate colors and magnitudes for the vast majority of RASS counterparts, and even the spectroscopic portion of SDSS, in which the $\sim$45 minute exposure times are set primarily to provide acceptable signal for the galaxies in the large-scale structure survey, will yield excellent quality spectra for the large majority of counterparts, permitting confident identifications and in-depth subsequent analyses.

Additionally, the full RASS/SDSS area is also covered by the NVSS and/or FIRST 20 cm radio surveys (Condon et al. 1998; Becker, White, & Helfand 1995). Thus, radio information is also available for virtually *every* interesting RASS/SDSS object.

The final part of the good match between RASS and SDSS is a consequence of the modest surface density of RASS sources on the sky—commonly, a few sources per square degree. A typical SDSS spectroscopic field of about 7 deg^2 thus has $\sim 10^1$ RASS sources, and therefore $\sim 10^4$ RASS sources in the ultimate SDSS sky coverage can be targeted for at least one spectroscopic observation, while only diverting 1% of the fibers from other SDSS scientific programs.

3. AUTONOMOUS SELECTION OF CANDIDATE OPTICAL COUNTERPARTS FOR SDSS SPECTRA

As noted above, a subset of objects of special interest in the SDSS imaging are slated for follow-up SDSS spectroscopy; objects are selected from the imaging database via various algorithms that comprise the SDSS "target selection" pipeline software (Stoughton et al. 2002). As part of that target selection pipeline, we have implemented algorithms aimed to specifically select candidate *ROSAT* counterparts for automated SDSS spectra. Optical objects in the SDSS photometric catalogs are automatically cross-correlated with objects in the RASS X-ray catalogs (Bright and Faint Source). Those SDSS optical objects within 1′ of the X-ray source positions are initially flagged (with a database flag "rosatMatch" having value >0) as potential positional matches in the imaging catalogs and considered further, though not all will receive follow-on SDSS spectra as we detail below.

As our eventual goal is the optical identification of $\sim 10^4$ RASS X-ray sources (a sample approximately an order of magnitude larger than previous efforts), we emphasize SDSS spectroscopic follow-up of that subset of the cataloged RASS sources that have the highest X-ray detection likelihoods (a maximum likelihood measure of the RASS X-ray source significance; see Voges et al. 1999). In the RASS/SDSS target selection algorithm, the minimum X-ray detection likelihood parameter is currently set to ≥ 10; this cut, imposed on the RASS catalog, yields the desired highest significance $\sim 10^4$ X-ray sources in the ultimate joint RASS/SDSS sky coverage.

While it would be optimal to take optical spectra of all objects within each such RASS error circle, this is not feasible in practice for several reasons. First, the minimum allowed spacing between SDSS spectroscopic fibers is 55″, and most error circles will be sampled spectroscopically on only a single occasion during the course of the entire SDSS survey. Second, the SDSS imaging data extend beyond $m \sim 22$, and therefore the faintest optical images detected are significantly fainter than the SDSS spectroscopic limits. A compromise is made to generally aim for taking an SDSS spectrum of a single optical object in each RASS error circle (with X-ray maximum-likelihood value ≥ 10) covered by SDSS. The optical object chosen for SDSS spectroscopy in each RASS circle must also be brighter than $m < 20.5$ (more

specifically, g, r, or $i < 20.5$); this is the magnitude limit for good quality SDSS spectra of emission-line objects in the typical 45 minute spectroscopic exposure times. There is also a bright limit of $m > 15$, needed to avoid spectroscopic cross talk between nearby multiobject fibers.

An additional complication is that, for technical reasons, photometric measures for all SDSS optical objects within each RASS circle may not generally be *intercompared* with one another at the stage when algorithmically selecting targets for SDSS optical fiber spectroscopy.[18] Thus, rather than using the SDSS multicolor imaging data to select the "best" candidate optical counterpart in each RASS circle for a spectrum, we instead (at the target selection stage) must independently assess the quality of each optical object in the RASS circle on an absolute scale, without knowledge of (or direct comparison with) any other positionally consistent optical objects.

Our approach is thus to assign every SDSS optical object (imaged at the time of "target selection") within the RASS circle to a broad priority-bin grade (A, B, C, D) for optical spectroscopy. These priority bins are based on typical ratios of X-ray–to–optical flux for various classes of known X-ray emitters, at a typical limiting RASS X-ray flux of a few times 10^{-13} ergs s^{-1} cm^{-2}, and are used to gauge identification likelihoods and hence assign spectroscopic priorities for SDSS candidate optical counterparts. SDSS optical magnitudes, colors, and morphology parameters, as well as FIRST radio data, serve as proxies at this stage for the likely object class.

Among the various possible priority bins for *ROSAT* counterpart identifications, we have chosen objects having a triple positional coincidence between a RASS X-ray source, an SDSS optical object, and a FIRST radio source, for highest priority for SDSS optical spectra; the SDSS object and FIRST source must match to within 2″ (which we note may miss some radio sources with complex morphology). As mentioned above, virtually 100% of the SDSS area will also be covered by the FIRST 20 cm radio survey, although the relevant FIRST catalogs may not always have been available when the SDSS target selection software was actually run. The cross-correlation with FIRST catalogs (also done automatically) is mainly intended to ensure sensitivity to BL Lac objects and other X-ray/radio–emitting quasars, but this algorithm also finds, for example, radio galaxies (isolated and in clusters). These highest priority triple-waveband RASS/SDSS/FIRST coincidences are flagged as "ROSAT_A" objects by the target selection pipeline software and indicated as such in the SDSS database.

Objects in RASS error circles with unusual SDSS colors indicative of AGNs and quasars (but lacking FIRST detections) are given next priority for SDSS optical spectra. Simple UV-excess selection $u-g < 0.6$ built into the RASS/SDSS target selection module, as well as far more sophisticated approaches (Richards et al. 2002; Newberg & Yanny 1997) looking for outliers in the full SDSS four-dimensional color space, are consulted in assigning objects to this potential AGN class. All such second-highest priority potential spectroscopic targets are flagged as "ROSAT_B" by the target selection algorithm module. In fact, more than 90% of the confirmed RASS/SDSS quasars/AGNs are selectable by the simple UV-excess criterion (see Fig. 1); this is not surprising, as X-ray selection at the RASS flux limits has long been known to favor low-luminosity quasars and related AGNs at low redshift (e.g., Margon, Chanan, & Downes 1982). These color-outlier selections (especially because of the sensitivity to UV excess) also sometimes yield identifications that, upon examination of the SDSS spectra, turn out to be X-ray–emitting cataclysmic variables, white dwarfs, etc. (The latter classes are the topics of other SDSS papers.)

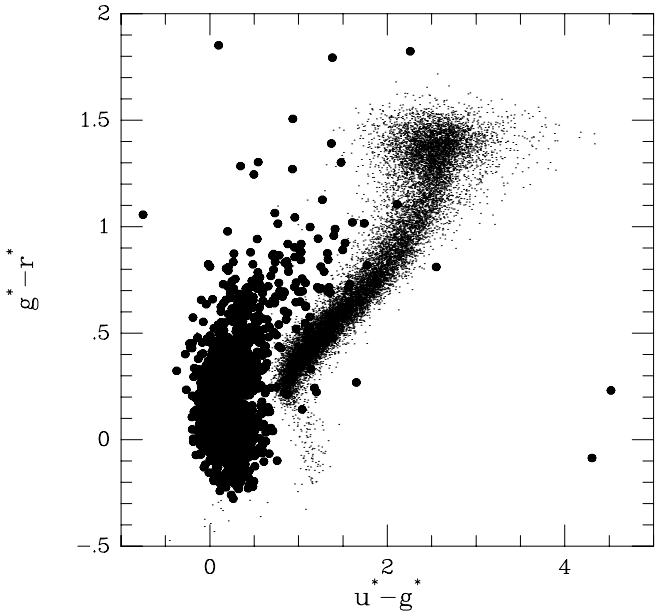

FIG. 1.—Odd-colored SDSS optical objects (as well as coincidences with FIRST radio sources) and positionally coincident with RASS X-ray positions are given high priority for SDSS spectroscopic follow-up. The SDSS colors of 1225 spectroscopically confirmed quasars and other X-ray–emitting AGNs in this initial sample are overplotted (*large filled circles*) for comparison on the locus of 10,000 anonymous SDSS stellar objects (*small points*). Note the clean color separation of the large majority of the confirmed quasar/AGN identifications. (For simplicity of display, three very red in $u-g$ objects [formally with PSF colors $u^*-g^* > 5$] are not shown. These objects are extremely faint in u, so their precise $u-g$ colors are uncertain.)

The third broad priority bin includes a varied set of somewhat less likely or less interesting, but still plausible, identifications, including bright stars and galaxies (currently $r < 16.5$ and $r < 17.5$, respectively; but also recall the general spectroscopic *bright* limit of $m > 15$), unusually blue galaxies ($g-r < 0.2$), and moderately blue stars ($u-g < 1.1$). These medium-priority spectroscopic targets are flagged as "ROSAT_C" by the target selection pipeline module.

The fourth broad priority bin includes any object bright enough (but not too bright) for optical spectroscopy that falls within the RASS circle. Objects in this class are flagged as "ROSAT_D" by the target selection pipeline, and most are rather unlikely to be the proper identifications; on the other hand, it is important to allow for this group as well, lest our biases based on past studies preclude discovery space for new classes of X-ray emitters.

[18] For example, in an extreme case it could even be that early SDSS optical imaging covers only some portion of a given X-ray error circle, while optical imaging coverage of the remainder of the X-ray error circle will not be completed until very late in the survey.

Among the confirmed quasars/AGNs cataloged in this paper, selected for possible SDSS spectra by virtue of their interest as potential RASS identifications, the great majority were (as expected) assigned to either—or sometimes both—ROSAT_A and ROSAT_B categories. When considering just the highest priority bin assigned: 16% were assigned ROSAT_A, 76% were assigned ROSAT_B, 3% ROSAT_C, and 5% ROSAT_D.

One subtlety of RASS/SDSS target selection is that because of the restriction noted above that optical objects within an X-ray error circle may *not* have their photometry inter-compared beforehand to pick the "best" candidate, a situation may still arise in which, for example, both a ROSAT_A and a ROSAT_D object, well separated in the same X-ray error circle, could otherwise still both be assigned an SDSS spectroscopic fiber. In order to avoid wasting the second fiber in such a case, a trick is now imposed that effectively restricts spectroscopy in most cases to only a single SDSS candidate in each X-ray error circle: currently, only optical candidate counterparts within radius $27\farcs5 = 55''/2$ offset from the X-ray source are ultimately allowed for selection for spectroscopy by the target selection software module devoted specifically to RASS/SDSS. The minimum $55''$ mechanical spacing between spectroscopic fibers then ensures that only a single SDSS optical object within the X-ray error circle will actually receive a RASS/SDSS spectroscopic fiber: one in the highest priority bin offset less than $27\farcs5$ from the X-ray source. (If there are multiple SDSS objects of the same priority—e.g., two SDSS objects within $27\farcs5$ of a RASS source, both having priority class ROSAT_A—then one is chosen at random for SDSS spectroscopy).

For aid in database bookkeeping, we have added an additional flag "ROSAT_E," that is now also assigned at the target selection stage to indicate an SDSS optical object of potential interest that is unsuitable for follow-up SDSS spectroscopy for any reason. For example, this flag might call attention to an SDSS object of interest outside the $27\farcs5$ radius offset discussed in the preceding paragraph (but within $1'$ of the RASS source position), or one too bright or too faint for SDSS spectroscopy, or one matching a RASS source with X-ray detection likelihood below 10, etc. (Note also that an SDSS object may receive more than one ROSAT target selection flag, e.g., one with ROSAT_A and ROSAT_E flags set might indicate a triple radio/optical/X-ray match, but one not suitable for SDSS spectra for some reason, etc.). We added the ROSAT_E flag during the early phases of SDSS commissioning, but after early target selection was already underway; however, this late addition complicates the bookkeeping on only about 10% of the objects discussed in this paper (and of course that fraction will decrease, as the sample expands).

The actual SDSS spectroscopic targeting situation is even somewhat more complex than described here (see Stoughton et al. 2002 for additional details). First, the target selection algorithms for each of the various other SDSS spectroscopic follow-up categories—quasars, galaxies, stars, serendipity objects, as well as *ROSAT* candidates—were under refinement in the early "commissioning" phases of SDSS. Secondly, objects that are part of the SDSS optical samples to obtain (ultimately) 10^6 spectroscopically observed galaxies and 10^5 confirmed quasars are actually assigned their spectroscopic fibers first via a sophisticated "tiling algorithm" (Blanton et al. 2003), before *any* consideration is given to potential RASS targets. For example, an SDSS object selected as a QSO candidate by the *quasar* target selection algorithm will very likely receive a spectroscopic fiber (and, e.g., even when the *ROSAT* algorithm flags it as ROSAT_E). Indeed, the following SDSS optical objects are nearly guaranteed to receive an SDSS spectroscopic fiber independent of X-ray emission: all galaxies to $r < 17.77$ (Petrosian magnitude), almost all SDSS point-spread function (PSF) objects to $i < 19.1$ with colors indicative of quasars, and almost all FIRST radio sources with optical PSF-morphology to $i < 19.1$. A common benefit is that the number of distinct SDSS fibers needed specifically for RASS sources is thereby further decreased because of the large fraction—about 80%—of RASS identifications that ultimately prove to be AGNs and which were already independently targeted for spectroscopy by the SDSS *quasar* target selection algorithms (before the algorithms specifically aimed at RASS candidates ever come into play). Moreover, the *quasar* target selection algorithms are not confined only to picking objects within the $27\farcs5$ offset restriction imposed on RASS/SDSS targets, so they can additionally sample counterparts throughout the full $1'$ X-ray error circles. Conversely though, a random galaxy targeted at high priority merely because it is part of the main SDSS galaxy redshift-survey sample, and falling by chance in a RASS error circle, may occasionally *exclude* another high-priority *ROSAT* target from any possibility of receiving a spectroscopic fiber. This is merely due to the $55''$ minimum fiber spacing.

The net effect is that RASS/SDSS target selection, both in general and also specifically for the objects cataloged in this paper, cannot guarantee "completeness." However, in practice we expect that the spectroscopic sample will ultimately prove to be reasonably complete at least for most classes of X-ray–emitting quasars and AGNs with $15 < m < 19$. Within the $27\farcs5$ offset from the RASS sources, such optical targets may be chosen for spectroscopy by both the quasar and the *ROSAT* target selection categories (and at larger positional offsets, about 80% of X-ray–emitting quasars/AGNs like those discussed herein may still be selected by the *quasar* target selection algorithms.)

Despite the limitations on completeness, examination of the very high quality SDSS spectroscopy (e.g., see Fig. 2) confirms that these target selection algorithms that choose odd-colored optical objects and/or radio sources within RASS error circles are highly efficient at locating X-ray–emitting quasars/AGNs. For example, objects selected by the ROSAT_A and/or ROSAT_B algorithms applied to the SDSS imaging data are confirmed to be X-ray–emitting AGNs conservatively more than about 75% of the time, upon examination of the follow-up SDSS spectra; in fact, approximately 85% of the spectra in these two algorithm categories are those of very likely quasars/AGNs (and constitute the catalogs presented herein), but a few percent of these may be chance superpositions unrelated to the X-ray sources as we discuss in § 6, and a few percent reflect slightly more speculative spectral classifications/identifications (the Seyfert 2 candidates discussed near the end of § 4.2, a handful of objects among the BL Lac candidates discussed in § 4.3, and a few dozen of the objects among

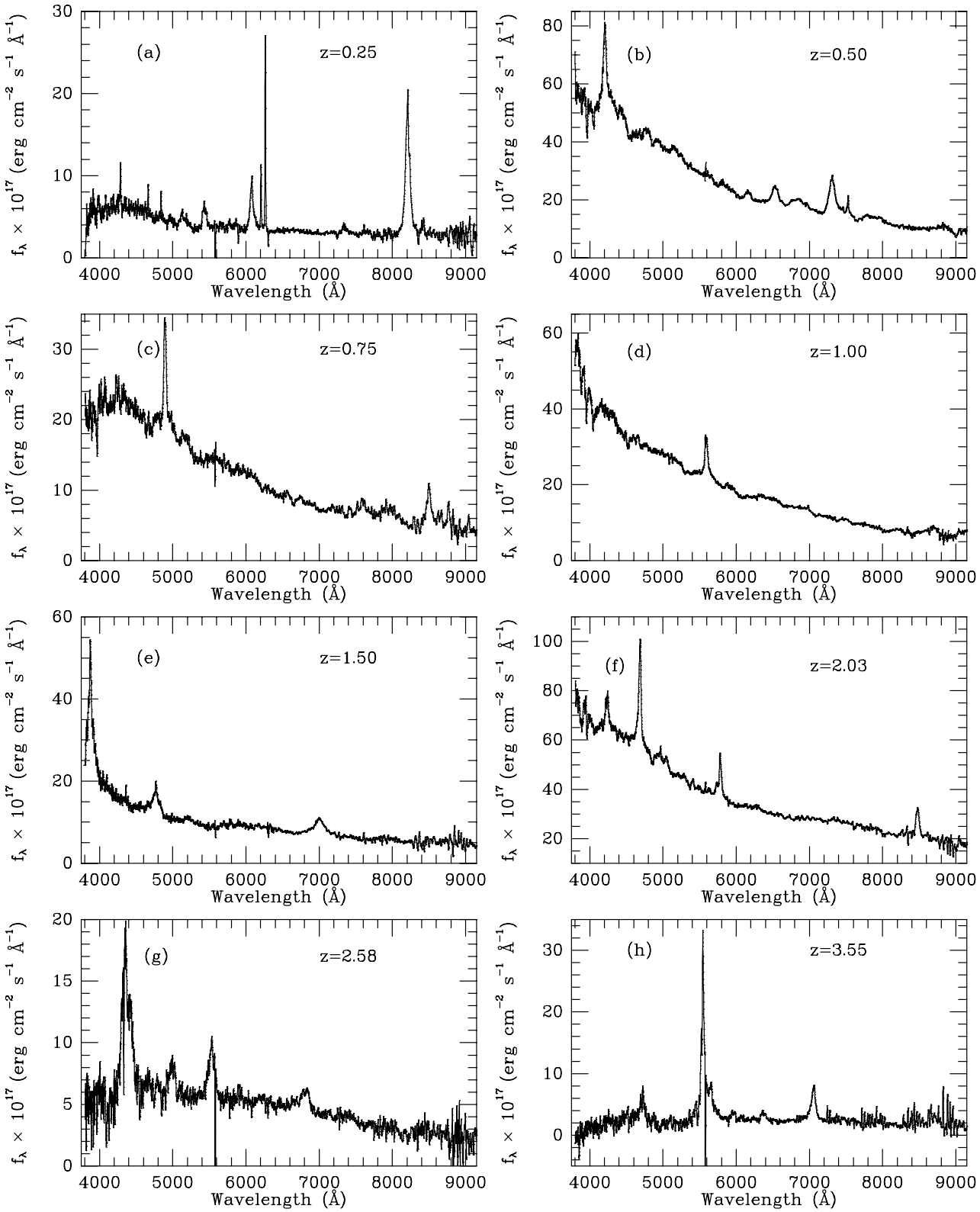

FIG. 2.—Example SDSS optical spectra for confirmed RASS/SDSS X-ray–emitting quasars/AGNs with (mainly) broad permitted emission, as discussed in § 4.1. Shown are spectra for typical objects covering a range of redshift from 0.25 to 3.5. All 964 such objects cataloged/discussed in § 4.1 have similar high-quality SDSS spectroscopy. (*a*) SDSS J233024.73+011602.3; (*b*) SDSS J234440.03−003231.6; (*c*) SDSS J103245.16+644154.2; (*d*) SDSS J170035.42+632522.6; (*e*) SDSS J172424.36+571531.0; (*f*) SDSS J150837.11+604955.8; (*g*) SDSS J155104.23+521637.7; (*h*) SDSS J125227.28+001001.9.

the large sample of NLSy1's discussed in § 5.1). The efficiency of spectroscopic identifications may also be somewhat larger than quoted above for the ROSAT_A and ROSAT_B categories, as these same algorithms also yield 8% other sorts of galaxies (4% are galaxies with comparatively weak/narrow or no optical emission, plus 4% radio galaxies having bland optical spectra), 3% stars, most of which are either white dwarfs or cataclysmic variables (CVs), and 4% of the spectra that are either ambiguous or of too low signal-to-noise ratio (S/N) to definitively classify. Some fraction of these additional objects (e.g., nearly *all* of the CVs—which are already cataloged as likely X-ray sources in other SDSS papers by Szkody et al. 2002, 2003) are also plausible additional RASS identifications, but are not included, nor counted as successes, in the discussions of the current AGN paper.

4. INITIAL CATALOG OF 1200 X-RAY–EMITTING AGNs FROM RASS/SDSS

In this section, we present initial results toward the ultimate goal of a sample of $\sim 10^4$ well-characterized optical identifications of RASS X-ray sources. The emphasis in this installment of the RASS/SDSS catalog is on our initial set of more than 1200 X-ray–emitting quasars and other sorts of AGNs; as discussed below in § 6, for these AGNs the identifications are secure at least in a statistical sense. The comprehensive range of Galactic and extragalactic X-ray identifications will be discussed in upcoming papers related to the SDSS Data Release 1 and beyond (e.g., Voges et al. 2003). Other *ROSAT* results especially from the SDSS Early Data Release (EDR), bearing on various specific X-ray–emitting classes include: cataclysmic variables (Szkody et al. 2002, 2003), clusters of galaxies (Sheldon et al. 2001), EDR narrow-line Seyfert 1's (Williams, Pogge, & Mathur 2002), and EDR quasars (Schneider et al. 2002; Vignali, Brandt, & Schneider 2003a).

4.1. *Quasars and Other AGNs with* (*Predominantly*) *Broad Permitted Lines*

In Tables 1 and 2 we present a catalog of 964 spectroscopically confirmed RASS/SDSS quasars and closely related AGNs having (predominantly) broad permitted emission lines; all have optical positions within 1′ of RASS X-ray sources. We include under this present category of quasars and other "broad-line" AGNs all such RASS/SDSS objects whose spectra show characteristic strong optical emission lines of AGNs, with broad permitted emission having velocity widths in excess of 1000 km s^{-1} FWHM. For low-redshift objects in the range out to about $z < 0.4$ where Mg II λ2800 is not yet accessible, we rely on the Hβ emission line to make this velocity-width determination; for higher redshift AGNs, we merely consider the FWHM of the broadest line observed within the SDSS spectroscopic coverage. Note that, aside from luminosity and data quality criteria, this category is defined similarly to that of the Schneider et al. (2002) EDR quasar catalog. However, we avoid any a priori luminosity cuts, and so these first tables include not only most quasars, but also most Seyfert 1's, many Seyfert 1.5's, and even many of such unusual but interesting classes as NLSy1's.

Nearly all (about 98%) of these broad-line AGNs were selected for spectroscopy by either the *ROSAT* or the quasar target selection algorithms (or both as discussed above) applied to the SDSS imaging database.[19] This catalog reflects objects having follow-up SDSS spectroscopy parameters stored within a database accessible to the SDSS collaboration (for internal reference, we refer to this as the "Chunk 8 database") as of early 2002; that database included information from 269 (distinctly numbered) spectroscopic plates, of which 251 are in common with spectroscopic plates included in the most recent public data release (Data Release 1; Abazajian et al. 2003). All objects have confirming, high-quality SDSS optical spectra; see Fig. 2 for representative examples. About 20% of these objects were both already cataloged as quasars/AGNs and also had redshifts reliably established prior to SDSS, and the bulk are newly identified as X-ray–emitting AGNs from combined RASS/SDSS data. Other objects were previously cataloged in Bade et al. (1998a) and related lists but lacked secure identifications in their low-resolution grism/prism spectral data. (See also Margon et al. 2000, Voges et al. 2001, Schneider et al. 2002, Williams et al. 2002, and Vignali et al. 2003a for discussions of various subsets of the several hundred AGN identifications available earlier from the EDR.) In this paper, Table 1 catalogs mainly empirical characteristics of the 964 X-ray–emitting broad-line quasar/AGN counterparts obtained from SDSS, while Table 2 provides other derived information discussed herein. In both tables, objects are ordered according to the J2000 right ascension of the RASS X-ray source.

In Table 1, emphasizing observed parameters, column (1) provides the RASS X-ray source position (J2000) using right ascension/declination nomenclature. Column (2) similarly provides the optical position/nomenclature (J2000) of the suggested quasar/AGN counterpart as measured from SDSS data; the optical astrometry is accurate to better than 0″.1 (Pier et al. 2003). Columns (3)–(7) provide optical photometry in the five SDSS passbands (e.g., Fukugita et al. 1996) in the asinh AB system (Lupton, Gunn, & Szalay 1999); as the final SDSS photometric calibrations were not completed at the time this project began, the PSF magnitudes in Table 1 are denoted with an asterisk, and the estimated calibration uncertainties are on the order of a few percent. Column (8) provides the value of the SDSS imaging parameter "objc_type," a commonly used and reliable SDSS measure of optical morphology (see Stoughton et al. 2002 for more details); objc_type = 6 indicates stellar/unresolved optical morphology, while objc_type = 3 indicates an extended/resolved (i.e., galaxy) morphology. Column (9) provides the redshift as measured from the SDSS spectra; in most cases the quoted redshift is that provided by the SDSS spectroscopic pipeline, but we have confirmed all redshifts by an independent manual/by-eye check, and agreement in most cases (except for a handful

[19] As an additional check on the autonomous target selection algorithms discussed above, we have also considered post facto (and cataloged here as AGNs where appropriate) all SDSS objects with an optical spectrum that falls within 1′ of a RASS source and independent of whether or not it was actually selected by the *ROSAT* target selection algorithms described in the preceding section. For this additional check we externally cross-correlated with the RASS catalogs the positions of ~200,000 optical objects having spectral information incorporated into the SDSS database as of early 2002 and examined all 3141 resulting SDSS spectra. This additional check confirms that the autonomous RASS/SDSS target selection pipeline algorithms are working as anticipated, and are not missing any substantial set of X-ray–emitting AGNs.

TABLE 1

OBSERVED PARAMETERS OF BROAD-LINE RASS/SDSS AGNs

RASS X-Ray Source (RXS J) (1)	SDSS Optical Counterpart (SDSS J) (2)	u^* (3)	g^* (4)	r^* (5)	i^* (6)	z^* (7)	Optical Morph. (8)	Redshift (9)	X-Ray Count Rate (10)	X-Ray Exp. Time (11)	X-Ray HR1 (12)	X-Ray HR2 (13)	X-Ray–like (14)	f_x ($\times 10^{13}$) (15)
000011.9+000223.....	000011.96+000225.2	17.83	17.58	17.69	17.65	17.66	6	0.479	0.0219	364	-0.01	-1.00	9	2.21
000250.8+000824.....	000251.60+000800.5	19.98	18.95	18.11	17.64	17.48	3	0.107	0.0410	388	-0.32	0.09	9	4.10
000611.9−010648.....	000608.04−010700.8	18.95	18.54	18.44	18.43	18.55	6	0.948	0.0243	394	-0.25	-0.66	8	2.49
000709.8+005328.....	000710.01+005329.0	17.18	16.87	16.64	16.69	16.05	6	0.316	0.1045	405	0.07	0.04	62	10.12
000813.3−005752.....	000813.22−005753.3	18.97	18.29	17.66	17.08	16.89	3	0.139	0.0508	394	-0.02	0.02	27	5.14

NOTES.—Table 1 is presented in its entirety in the electronic edition of the Astronomical Journal. A portion is shown here for guidance regarding its form and content.

TABLE 2
DERIVED PARAMETERS OF BROAD-LINE RASS/SDSS AGNs

RASS X-Ray Source (RXS J) (1)	SDSS Optical Counterpart (SDSS J) (2)	g_o^* (3)	Redshift (4)	f_x^c ($\times 10^{13}$) (5)	log L_x (6)	log l_{opt} (2500 Å) (7)	log l_x (2 keV) (8)	α_{ox} (9)	Comments (10)
000011.9+000223.....	000011.96+000225.2	17.46	0.479	5.43	44.76	30.29	26.22	1.56	LBQS 2357−0014
000250.8+000824.....	000251.60+000800.5	18.83	0.107	10.03	43.49	28.33	24.95	1.30	
000611.9−010648.....	000608.04−010700.8	18.40	0.948	6.21	45.60	30.58	27.06	1.35	Radio
000709.8+005328.....	000710.01+005329.0	16.75	0.316	24.18	44.95	30.17	26.42	1.44	Radio, LBQS 0004+0036
000813.3−005752.....	000813.22−005753.3	18.17	0.139	12.70	43.84	28.84	25.31	1.36	

NOTES.—Table 2 is presented in its entirety in the electronic edition of the Astronomical Journal. A portion is shown here for guidance regarding its form and content.

that we have corrected in the tables based on our manual measures) was to within 0.01 in z. The remaining columns of Table 1 emphasize the X-ray data on the broad-line quasars/AGNs and are derived directly from the RASS catalogs (e.g., see Voges et al. 1999, 2000). Column (10) provides the RASS X-ray source count rate (counts per second) in the 0.1–2.4 keV broadband, corrected for vignetting. Column (11) gives the RASS exposure time in seconds. Columns (12) and (13) provide X-ray hardness ratios as measured from several X-ray bands (see Voges et al. 1999). Column (14) is the X-ray source detection likelihood (a maximum likelihood measure of source significance). Column (15) gives the estimated X-ray flux in the 0.1–2.4 keV band, as observed, i.e., without corrections for absorption in the Galaxy; we used the PIMMS (Portable, Interactive, Multi-Mission Simulator) software to convert RASS count rates into X-ray fluxes, assuming a power-law X-ray spectrum with energy index $\alpha_x = 1.5$ typical of (low redshift) quasars in the RASS passband (e.g., see Schartel et al. 1996).

In Table 2, we present further catalog information on the 964 broad-line RASS/SDSS AGNs, but now also emphasizing derived quantities used herein. For a more convenient cross-reference we repeat some relevant information included in Table 1. Columns (1) and (2) repeat, respectively, the RASS X-ray source and suggested optical counterpart name/position. Column (3) provides the extinction-corrected g-band PSF magnitude, corrected according to the reddening maps of Schlegel, Finkbeiner, & Davis (1998). Column (4) repeats the redshift from SDSS spectroscopy. Column (5) is the X-ray flux (in units of 10^{-13} ergs s^{-1} cm^{-2}) in the 0.1–2.4 keV band, now corrected for absorption within the Galaxy, and with absorbing columns estimated from the N_H column density measures of the Stark et al. (1992) 21 cm maps. Columns (6), (7), and (8) give the logarithms of, respectively, inferred broadband (0.1–2.4 keV) X-ray luminosity (in units of ergs per second), monochromatic UV/optical luminosity (in units of ergs s^{-1} Hz^{-1}) at a frequency corresponding to rest frame 2500 Å and monochromatic soft X-ray luminosity at 2 keV; we adopt values of $H_0 = 70$ km s^{-1} Mpc^{-1}, $\Omega_M = 0.3$, and $\Omega_\Lambda = 0.7$ for deriving the luminosities in Table 2. In converting from corrected broadband (X-ray 0.1–2.4 keV and optical g-band) flux to luminosities, we again assume an X-ray power-law spectrum with energy index $\alpha_x = 1.5$ and an optical power-law with energy index $\alpha_o = 0.5$. Column (9) lists α_{ox}, the slope of a hypothetical power law (in energy) from the UV/optical to X-ray (i.e., connecting 2500 Å and 2 keV). Column (10) provides brief comments, e.g., noting selected objects that are radio sources, including one alternate name for objects whose spectral classification and accurate redshift were both available (in catalogs/papers incorporated into the NASA/IPAC Extragalactic Database) prior to SDSS, noting the ~1% of the cases in which two of our cataloged AGNs fall within the same RASS error circle (latter denoted as "ambigID" in the comments), etc.

4.2. *X-Ray–emitting AGNs Having Narrower Permitted Emission*

In addition to the predominantly broad-line (FWHM > 1000 km s^{-1}) AGNs discussed above in § 4.1, we also examined and approximately classified the spectra of all other extragalactic emission-line objects in RASS error circles observed spectroscopically by SDSS. Primarily, this was done to ensure fuller sampling of the specific possible X-ray–emitting AGN subclasses such as NLSy1's, Seyfert 1.5's, Seyfert 1.8's, and Seyfert 1.9's that have optically observable broad-line regions; i.e., objects very closely related to classic quasars and Seyfert 1's, but which may be observed to have narrower permitted-line components as well. In addition, we have also extended this subset to include Seyfert 2 candidates, i.e., AGNs whose optical emission is nearly entirely dominated by a narrow-line region. The additional AGNs cataloged in this section are exclusively at low redshift, so again it is initially the Hβ line width/profile that we consult. That is, the objects discussed in this section all have FWHM(Hβ) < 1000 km s^{-1} based on a *naive* (and in many cases here, incorrect) line measure that assumes a single component to the line profile.

For classification as Seyfert 1.5 to Seyfert 1.8, we require the full width near the continuum level (FWZI) of the Hβ emission line to exceed 2500 km s^{-1}. Of course measurements near the continuum are problematic near Hβ, especially when Fe is strong, but except for the unusual case of some NLSy1's, we have also verified that the FWZI of the Hβ line exceeds that of the [O III] λ5007 emission in the same object by at least ~1000 km s^{-1}; hence each such object has a broad-line component substantially wider than is typical of its narrow-line region. The taxonomic classifications provided in this section are mainly intended as an aid in clarifying why these objects, although similar, did not satisfy the specific criteria discussed in § 4.1 for (predominantly) broad-line quasars and AGNs. To make the specific taxonomic subdivisions simple but more concrete, we label as Seyfert 1.5 those objects having *both* broad and narrow Hβ components and with relatively small [O III] λ5007 to Hβ flux ratios of $R < 3$ and label those with $R > 3$ as

Seyfert 1.8's; see Whittle (1992) for a similar subclassification scheme.[20] (The NLSy1's are discussed in more detail in § 5.1.)

We also select a number of low-redshift objects in RASS error circles, whose SDSS optical spectra show little or no evidence of broad Hβ, but which do appear to have a markedly broad Hα emission component. We refer to these (somewhat loosely) as Seyfert 1.9's; however, in low-S/N cases, weak broad Hβ may not be well measured or even recognized, so some of these are likely to really be Seyfert 1.5–1.8's. To help limit confusion in these "Seyfert 1.9" cases between truly broad Hα and those in which narrow Hα is merely blended with [N II] emission, as well as complications of contaminating late-type stellar continuum/absorption features in cases with substantial host-galaxy stellar light, we very conservatively limit our Seyfert 1.9 candidate list to include just those cases with very broad Hα, requiring FWZI(Hα) > 6000 km s^{-1}.

Finally, we also extend our catalog a little to include candidate X-ray–emitting Seyfert 2's and related AGNs. Possible identifications of Seyfert 2's, starbursts, and other narrow emission line galaxies as X-ray–emitting subclasses have been discussed in multiple papers most recently emphasizing deeper, higher spatial resolution and/or harder energy X-ray imaging surveys (e.g., Boyle et al. 1995; McHardy et al. 1998). However, in some cases subsequent improved follow-on optical spectroscopy has led to ultimate reclassifications (e.g., Halpern, Turner, & George 1999) into one of the categories already considered above, e.g., NLSy1, Seyfert 1.8, or Seyfert 1.9. Nonetheless, an extension to include X-ray–emitting Seyfert 2 candidates may be of interest for several reasons including the following: type 2 AGNs are sometimes invoked as significant contributors to the cosmic X-ray background, and nearby bright examples may be individually interesting if bona fide Seyfert 2's; and even if the candidates discussed herein are not confirmed as X-ray–emitting Seyfert 2's on closer scrutiny, this group might still serve to encompass some unusually subtle cases of X-ray–emitting Seyfert 1.8–1.9's, NLSy1's, etc. We select candidate Seyfert 2's from among the remaining narrow emission line galaxies, using AGN emission-line diagnostics that are founded on the oft-used BPT (Baldwin, Phillips, & Terlevich 1981) diagrams and criteria. We employ the specific criteria of Kewley et al. (2001) based on the relative line strengths of [O III] λ5007/Hβ, [N II] λ6583/Hα, and [S II] $\lambda\lambda$6717, 6731/Hα; the Kewley et al. criteria quantify regions in the [O III]/Hβ versus [N II]/Hα and [O III]/Hβ versus [S II]/Hα BPT diagrams populated by AGNs versus starbursts.[21]

We catalog in Tables 3 and 4 basic empirical and derived information for the additional 216 X-ray–emitting AGNs discussed in this section (194 with observed broad-line regions, plus 22 Seyfert 2 candidates). Tables 3 and 4 for these additional AGNs are analogous to Tables 1 and 2, respectively, presented in § 4.1. In Table 4, the comment column may include the subclass type, and we denote some especially uncertain classifications with a question mark (e.g., "Sy 2?"). Figure 3 shows selected SDSS spectra from objects in this second diverse set of X-ray–emitting AGNs (and see § 5.1 for further details on NLSy1's).

4.3. *BL Lac Candidates*

We have also examined our RASS/SDSS sample for BL Lac candidates, which (by the subclass definition) would, of course, not be found in the above samples of AGNs with prominent emission lines. Because of their rarity (only a few percent of the objects in current quasar catalogs) and unusual properties (nonthermal continua, with strong X-ray and radio emission and nearly featureless optical spectra, high polarization, marked variability, and possible "negative" evolution; e.g., Urry & Padovani 1995; Morris et al. 1991), large and well-defined samples of BL Lac objects are eagerly sought, but until recently have proved extraordinarily difficult to assemble. Their rarity demands large areal sky coverage, and yet their unusual spectral energy distributions and lack of strong spectral features often render traditional quasar/AGN optical selection incomplete and/or inefficient for BL Lac objects. Despite numerous attempts, until recently there were only a handful of homogeneous BL Lac samples of even modest size from which to study their remarkable characteristics.

Many recent efforts (e.g., Stocke et al. 1991; Perlman et al. 1996; Laurent-Muehleisen et al. 1997; Bade et al. 1998b) to obtain well-defined BL Lac samples utilize a combination of multiwavelength information from the X-ray, optical, and radio bands to obtain high selection efficiency. Stocke et al. (1991), Perlman et al. (1996), and others noted that BL Lac objects have distinctive multiwavelength flux ratios; e.g., BL Lac objects have unusually large f_x/f_{opt} ratios compared with other AGNs, and nearly all those cataloged that may confidently be called BL Lac objects are radio sources as well. We employ these same general approaches and criteria within our ROSAT_A target selection algorithm (as discussed in § 3) to obtain an initial list of RASS/SDSS BL Lac candidates. (We again also consider post facto all optical spectra of SDSS objects taken in the relevant RASS circles, to ensure our algorithms are not missing a significant subset.)

We find/recover 38 objects we consider as *probable* X-ray–emitting RASS/SDSS BL Lac objects. For all these higher confidence cases the following apply: (1) the SDSS optical object is within 1′ of a RASS source; (2) the SDSS object is also a positional match to a radio source (e.g., conservatively taken as less than 2″ in this initial study for matches to FIRST sources, or less than 20″ for matches to other radio catalogs); (3) our measures from the SDSS optical spectrum reveal no strong emission (EW < 4 Å); and (4) there is no Ca II H and K break/depression evident in the SDSS optical spectrum, or any such break present must be only very weak (quantitatively, the measured ratio of the galaxy's flux redward of any break to that blueward is required to be less than 1.33; see, e.g., Stocke et al. 1991 and Dressler & Schectman 1987). The latter criterion reflects the circumstance that X-ray–selected BL Lac objects sometimes have weak breaks, but not entirely featureless optical spectra (due to sometimes more pronounced starlight contamination from the host galaxies); of course, many of the RASS/SDSS BL Lac objects do indeed have approximately classically featureless optical spectra, as we show below. We also find/recover as *possible* BL Lac candidates seven

[20] We do not attempt here to subclassify cases like Seyfert 1.2, which is intermediate between Seyfert 1 and Seyfert 1.5.

[21] Except that we do not consider the relatively weak O I line in our Seyfert 2 classifications. See also Zakamska et al. (2003) and Kauffmann et al. (2003), who apply similar classification approaches to much larger *optical* samples of possible SDSS type 2 AGNs.

TABLE 3

OBSERVED PARAMETERS OF RASS/SDSS AGNS HAVING NARROWER PERMITTED EMISSION

RASS X-Ray Source (RXS J) (1)	SDSS Optical Counterpart (SDSS J) (2)	u^* (3)	g^* (4)	r^* (5)	i^* (6)	z^* (7)	Optical Morph. (8)	Redshift (9)	X-Ray Count Rate (10)	X-Ray Exp. Time (11)	X-Ray HR1 (12)	X-Ray HR2 (13)	X-Ray–like (14)	f_x ($\times 10^{13}$) (15)
002847.7+145142.....	002848.77+145216.3	19.66	18.88	18.44	17.98	17.71	3	0.089	0.0247	422	0.13	-0.69	14	2.80
003238.2−010056.....	003238.20−010035.2	18.90	18.25	17.84	17.41	17.22	3	0.092	0.0688	625	-0.10	0.46	33	6.50
003846.3+003430.....	003843.06+003451.7	19.82	18.43	17.95	17.67	17.32	3	0.043	0.0641	303	-0.39	0.77	18	5.38
004055.2+000039.....	004052.14+000057.2	18.37	18.20	18.04	18.11	17.88	6	0.405	0.0232	296	-1.00	0.00	8	1.97
004532.6−005807.....	004533.46−005808.8	18.78	18.56	18.32	17.97	18.04	6	0.138	0.0512	329	-1.00	0.00	14	4.88

NOTES.—Table 3 is presented in its entirety in the electronic edition of the Astronomical Journal. A portion is shown here for guidance regarding its form and content.

TABLE 4
DERIVED PARAMETERS OF RASS/SDSS AGN HAVING NARROWER PERMITTED EMISSION

RASS X-Ray Source (RXS J) (1)	SDSS Optical Counterpart (SDSS J) (2)	g_o^* (3)	Redshift (4)	f_x^c ($\times 10^{13}$) (5)	log L_x (6)	log l_{opt} (2500 Å) (7)	log l_x (2 keV) (8)	α_{ox} (9)	Comments (10)
002847.7+145142.....	002848.77+145216.3	18.59	0.089	7.57	43.19	28.26	24.66	1.38	Radio, Sy1.5
003238.2−010056.....	003238.20−010035.2	18.17	0.092	15.24	43.53	28.46	24.99	1.33	Sy1.5
003846.3+003430.....	003843.06+003451.7	18.36	0.043	11.64	42.71	27.70	24.17	1.36	Sy2?
004055.2+000039.....	004052.14+000057.2	18.09	0.405	4.30	44.47	29.88	25.93	1.51	NLS1
004532.6−005807.....	004533.46−005808.8	18.49	0.138	11.54	43.79	28.70	25.26	1.32	

NOTES.—Table 4 is presented in its entirety in the electronic edition of the Astronomical Journal. A portion is shown here for guidance regarding its form and content.

additional objects that are within RASS error circles and either satisfy the first three criteria (X-ray/radio sources with no strong optical emission), but just barely miss on the fourth criterion (two objects that have Ca II break flux ratios of between 1.33 and 1.40); or have too low an S/N in their SDSS optical spectra to claim the BL Lac spectral nature of criteria 3 and 4 with much confidence (three objects); or show approximately featureless SDSS spectra, i.e., that satisfy criteria 1, 3, and 4, but for which a close match has not been made to a radio source (two objects).

In the 1400 deg^2 of sky considered here then, a total of 45 candidate optical counterparts satisfy these criteria as probable or possible BL Lac objects, and basic information is provided for them in Tables 5 and 6 (which are analogous to Tables 1 and 2 for emission-line AGNs). In the comment column of Table 6, we use "zunc" to denote selected cases where the redshift from SDSS is highly uncertain, and the redshift is not available from (or is different in) the literature. (Of course, the quoted redshifts may also be lower limits on the actual BL Lac redshift, if the spectral absorption arises in foreground material rather than in the BL Lac host galaxy.) If a redshift is not obtained from the SDSS spectrum, nor already available in the literature, we adopt $z = 0.3$ (near the median of others in the sample) for estimating α_{ox} in Table 6; as this is essentially a ratio of luminosities, aside from precise

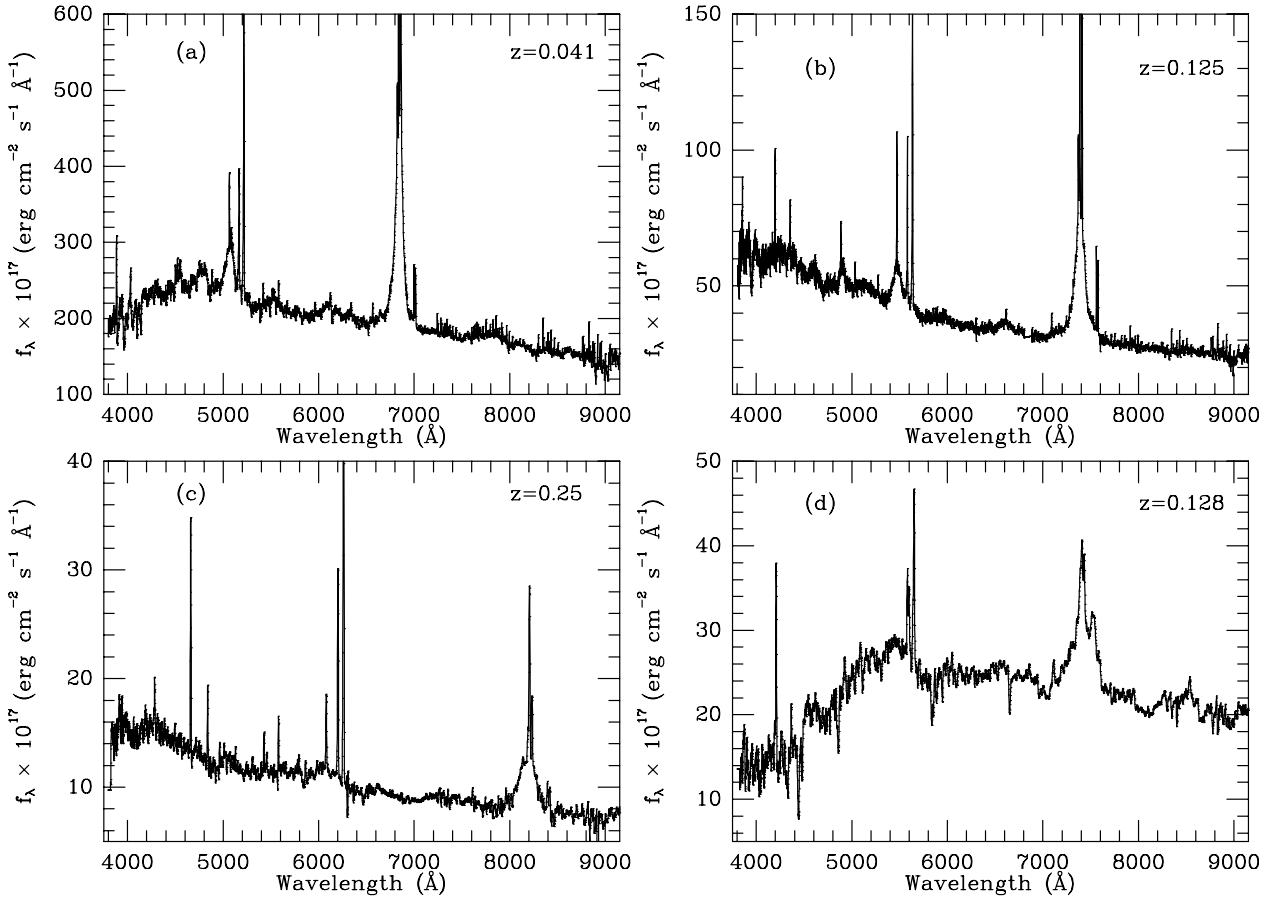

FIG. 3.—Example SDSS optical spectra for confirmed RASS/SDSS X-ray–emitting quasars/AGNs with both broad and narrower permitted emission components, chosen from the 216 objects cataloged/discussed in § 4.2. Shown are selected spectra for intermediate Seyfert types between Seyfert 1.5 and Seyfert 1.9. (*a*) SDSS J101912.57+635802.7; (*b*) SDSS J112841.60+633551.3; (*c*) SDSS J130550.51−012331.6; (*d*) SDSS J082133.60+470237.2.

TABLE 5

OBSERVED PARAMETERS OF RASS/SDSS BL LAC CANDIDATES

RASS X-Ray Source (RXS J) (1)	SDSS Optical Counterpart (SDSS J) (2)	u^* (3)	g^* (4)	r^* (5)	i^* (6)	z^* (7)	Optical Morph. (8)	Redshift (9)	X-Ray Count Rate (10)	X-Ray Exp. Time (11)	X-Ray HR1 (12)	X-Ray HR2 (13)	X-Ray–like (14)	f_x ($\times 10^{13}$) (15)
003514.9+151513.....	003514.72+151504.1	17.32	16.93	16.58	16.28	16.04	6	...	0.2358	359	0.35	0.25	235	27.08
020106.3+003400.....	020106.17+003400.2	19.35	19.06	18.43	18.14	17.83	3	0.298	0.3390	400	0.07	0.04	312	31.21
023812.9−092441.....	023813.67−092431.4	20.82	20.26	19.64	19.21	18.84	3	0.740	0.0345	224	0.72	0.42	17	3.32
030433.0−005409.....	030433.95−005404.6	19.15	18.86	18.50	18.15	17.90	6	0.513	0.0559	201	0.57	0.80	21	7.22
075436.4+391103.....	075437.07+391047.7	18.92	17.92	17.23	16.80	16.53	3	0.096	0.0344	422	0.06	-0.68	18	3.96

NOTES.—Table 5 is presented in its entirety in the electronic edition of the Astronomical Journal. A portion is shown here for guidance regarding its form and content.

TABLE 6
DERIVED PARAMETERS OF RASS/SDSS BL LAC CANDIDATES

RASS X-Ray Source (RXS J) (1)	SDSS Optical Counterpart (SDSS J) (2)	g_o^* (3)	Redshift (4)	f_x^c ($\times 10^{13}$) (5)	log L_x (6)	log l_{opt} (2500 Å) (7)	log l_x (2 keV) (8)	α_{ox} (9)	Comments (10)
003514.9+151513.....	003514.72+151504.1	16.66	...	74.47	...	...	...	1.27	RBS 0082
020106.3+003400.....	020106.17+003400.2	18.97	0.298	71.93	45.37	29.23	26.83	0.92	MS 0158.5+0019
023812.9−092441.....	023813.67−092431.4	20.16	0.740	7.88	45.41	29.63	26.87	1.06	RX J0238.2−0924, zunc
030433.0−005409.....	030433.95−005404.6	18.56	0.513	23.62	45.47	29.92	26.93	1.15	FBQS J0304−0054, zunc
075436.4+391103.....	075437.07+391047.7	17.74	0.096	10.91	43.42	28.67	24.89	1.45	RX J0754.6+3911

NOTES.—Table 6 is presented in its entirety in the electronic edition of the Astronomical Journal. A portion is shown here for guidance regarding its form and content.

K-corrections, the values of α_{ox} should be approximately correct in most cases. In Table 6, we denote the possible but less certain BL Lac candidates as "BL?" in the comment column. Example SDSS spectra of selected BL Lac candidates are shown in Figure 4.

About half of these objects have been previously reported in the literature as BL Lac objects or BL Lac–like objects, and some other objects were previously cataloged in Bade et al. (1998a) and related lists but lacked secure identifications in their low-resolution grism/prism spectral data. Even among the previously cataloged BL Lac objects, SDSS provides the first high-quality published optical spectra for many objects, and new spectroscopic redshift estimates (admittedly uncertain in some cases) for nine of the previously cataloged BL Lac objects. Where redshifts were available prior to SDSS, there is also usually good agreement with our SDSS measures, and in total two-thirds of the full sample of 45 have spectroscopic redshifts estimated from SDSS spectra, and/or other slit-spectra already published in the literature.

A few of the suggested BL Lac identifications may eventually prove to be misidentifications where a radio galaxy lies within an X-ray–emitting cluster or other group of galaxies (e.g., Rector, Stocke, & Perlman 1999). Others may

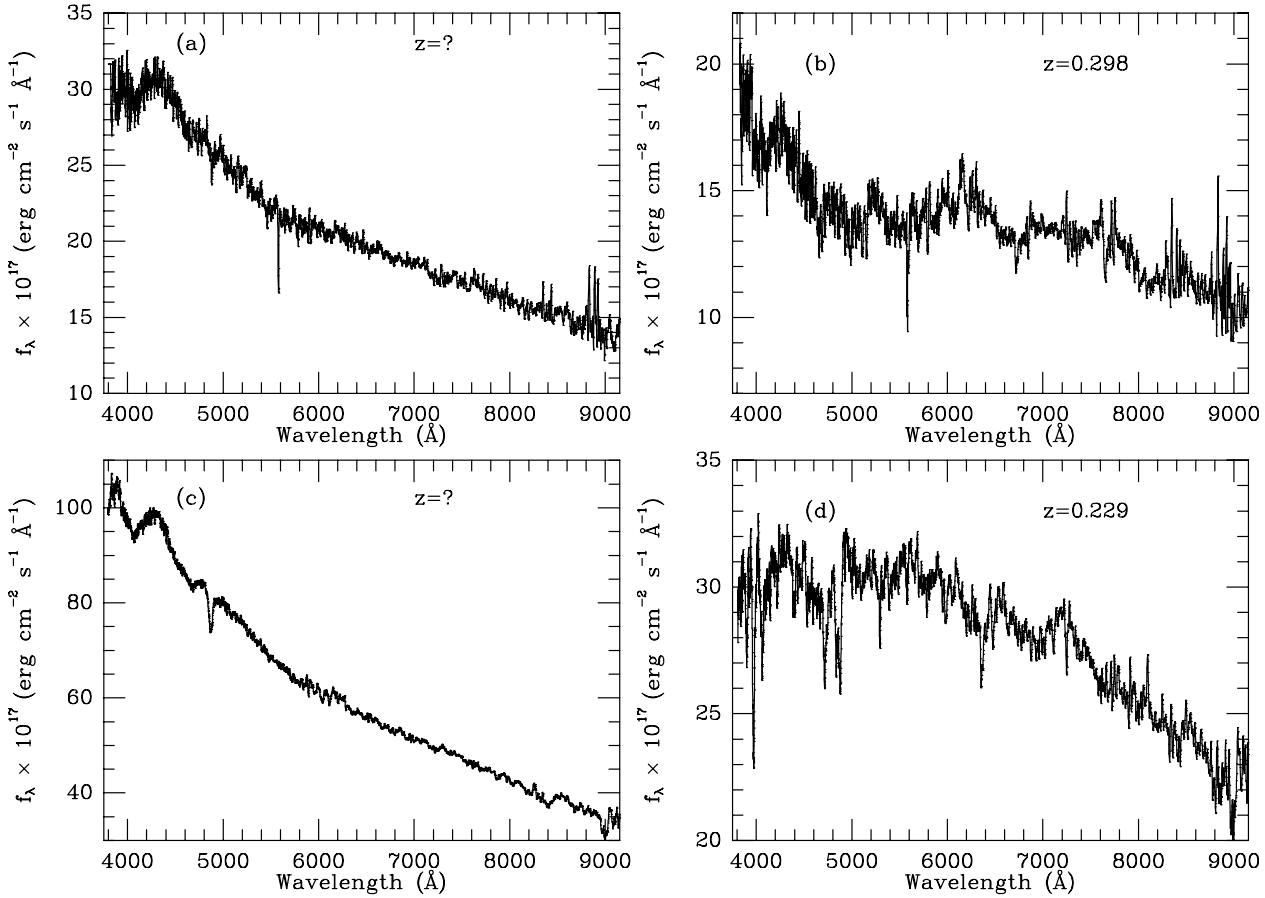

FIG. 4.—Example SDSS optical spectra of objects included in the RASS/SDSS sample of X-ray–emitting BL Lac objects and candidates; see text for discussion of selection. A total of 45 such candidates are presented in this initial RASS/SDSS catalog. (The apparent broad feature near 4300 Å is due to a systematic error in flux calibration of the spectra.) (*a*) SDSS J131106.47+003510.0; (*b*) SDSS J020106.17+003400.2; (*c*) SDSS J003514.72+151504.1; (*d*) SDSS J094542.23+575747.7.

prove to be stars on higher S/N or resolution spectroscopic follow-up; but it is worth recalling that all but a couple are both X-ray and radio sources, and so are more likely to be BL Lac objects than highly unusual X-ray/radio stars. As an additional precaution in the latter regard, we have also considered proper motion information. Collinge et al. (2003) are independently optically selecting SDSS BL Lac candidates using a lack of optical emission and a lack of significant proper motions (via comparison with the POSS) as their principal criteria. None of our 45 RASS/SDSS BL Lac candidates has significant proper motion (>20 mas yr^{-1}), e.g., suggesting little contamination by nearby hot white dwarfs, etc.

Thus, it seems likely that most of the BL Lac identifications are correct (see also § 6 below). In the ultimate RASS/SDSS joint sky coverage, we may thus predict with some confidence that we will be able to quantitatively define a sample of several hundred X-ray BL Lac candidates.

5. DISCUSSION OF OTHER RARE CLASSES AND INDIVIDUAL OBJECTS OF INTEREST

5.1. *Narrow-line Seyfert 1 Galaxies*

Among our RASS/SDSS AGNs (including objects discussed in both §§ 4.1 and 4.2), we identify from the SDSS spectra a total of 133 likely, and another 36 possible, X-ray–emitting NLSy1's. These objects are denoted by "NLS1" (likely) or "NLS1?" (possible) in the Comment columns of Tables 2 and 4. Gallo et al. (2003) are investigating this interesting subclass in detail from the current RASS/SDSS samples, and Williams et al. (2002) have recently discussed about 45 of these same objects independently selected from the EDR. The reader is thus referred to those far more extensive investigations. But briefly, these objects have unusually narrow permitted lines, though in other aspects are more similar to Seyfert 1's than Seyfert 2's; in the X-ray, these objects often show strong soft X-ray excesses and marked variability. A variety of explanations have been suggested for NLSy1's, including unusually low mass black holes, higher accretion rates relative to Eddington, nearly pole-on orientation, unusually thick broad-line regions, etc. (e.g., see recent reviews by Boller 2000 and Pogge 2000).

The 133 X-ray–emitting examples we label as reasonably confident cases all have low [O III] λ5007–to–Hβ flux ratios (we very conservatively restrict confident cases to $R < 1$), Hβ FWHM less than 2000 km s^{-1}, and strong optical Fe emission—representative characteristics of the NLSy1 class (e.g., Pogge 2000). The 36 less certain examples have either [O III]/Hβ ratios of $1 < R < 3$, weaker Fe, or lower quality and therefore more ambiguous SDSS spectra, etc. Among the one-third of the confident cases overlapping with Williams et al. (2002), we find good (~85%) agreement between our spectral classifications and theirs. Representative SDSS spectra for NLSy1's are shown in Figure 5.

5.2. *BAL QSOs*

Initial *ROSAT* studies (Green et al. 1995), and numerous subsequent follow-on studies, have shown that broad absorption line (BAL) QSOs as a class are weak emitters in soft X-rays. This deficiency at soft energies is usually interpreted as due to absorption of low-energy X-rays in BAL material of surprisingly high column densities, typically inferred equivalent to $N_H \sim 10^{22}$–10^{23} cm^{-2} (e.g., Green et al. 2001; Gallagher et al. 1999). There are several *possible* BAL QSOs or quasars with mini-BALs among the RASS/SDSS X-ray identifications discussed here, but these are not yet confirmed definitively. Shown in Figures 6*a* and 6*b* are the SDSS spectra of two such possible cases.

The numbers sampled thus far are tantalizing but conservatively still somewhat too small for definitive conclusions about the paucity of BAL QSOs among RASS/SDSS X-ray identifications. For example, SDSS spectral coverage yields good information on C IV BALs at redshifts above about $z > 1.7$, and our RASS/SDSS sample thus far includes about 50 such objects. If high-ionization BAL QSOs comprise on the order of order 10% of the quasar population, and if there were no bias against them in soft X-ray surveys, we would have expected to have found on the order of a half-dozen such BAL QSOs within the current sample. Results for low-ionization BAL QSOs are similar: low-ionization cases are probably present among only a few percent of the quasar population, so that once again only about a dozen might have been anticipated (even if "normal" in soft X-rays) within our current sample of about 450 RASS/SDSS quasars with $0.5 < z < 2.2$ (for which Mg II BALs might be easily identified from the SDSS spectra). Although the results for BAL QSOs are thus yet not quite definitive, future expansions of the RASS/SDSS sample—ultimately encompassing ~5 times as many objects as considered here—should allow rather stringent constraints on the incidence of BAL QSOs in soft X-ray surveys.

5.3. *Other Miscellaneous Interesting Subclasses/Objects*

In addition to NLSy1's with strong optical Fe emission discussed in § 5.1, there are another 71 objects with strong Fe emission (especially optical, but sometimes in UV), but with permitted line-widths in excess of the usual maximum of 2000 km s^{-1} considered applicable to the NLSy1 class. We denote these in Table 2 with "Fe" in the comments column. Example SDSS spectra are shown in Figures 6*c* and 6*d*.

In addition, there are also a half-dozen intermediate Seyfert objects that might be termed Seyfert 1.5–1.8, but for which the broad weak Hβ component appears markedly asymmetric (and/or complicated with Fe emission); Figure 6*e* shows one such example. There are additional objects that have strong and broad Mg II typical of classic quasars, but which if at slightly lower redshift might have been classified as about Seyfert 1.8 based on the Hβ line strength/profile; Figure 6*f* shows an example and one in which there appears to be both broad strong Hα and Mg II, but only rather weak broad Hβ.

There are many additional cases with unusual optical line profiles, including objects with very broad (~20,000 km s^{-1} FWZI) lines (Fig. 6*g*), as well as other AGNs with multiple-peaked line components (Fig. 6*h*). Many of the latter objects are included in the detailed study of Strateva et al. (2003).

6. DISCUSSION OF ENSEMBLE PROPERTIES AND RELIABILITY OF IDENTIFICATIONS

In the 1400 deg^2 of sky considered here, more than 1200 X-ray–emitting quasars or other AGNs are identified as likely RASS counterparts, each with uniform optical photometry and high-quality optical spectroscopy from SDSS. As discussed above, the SDSS optical spectra not

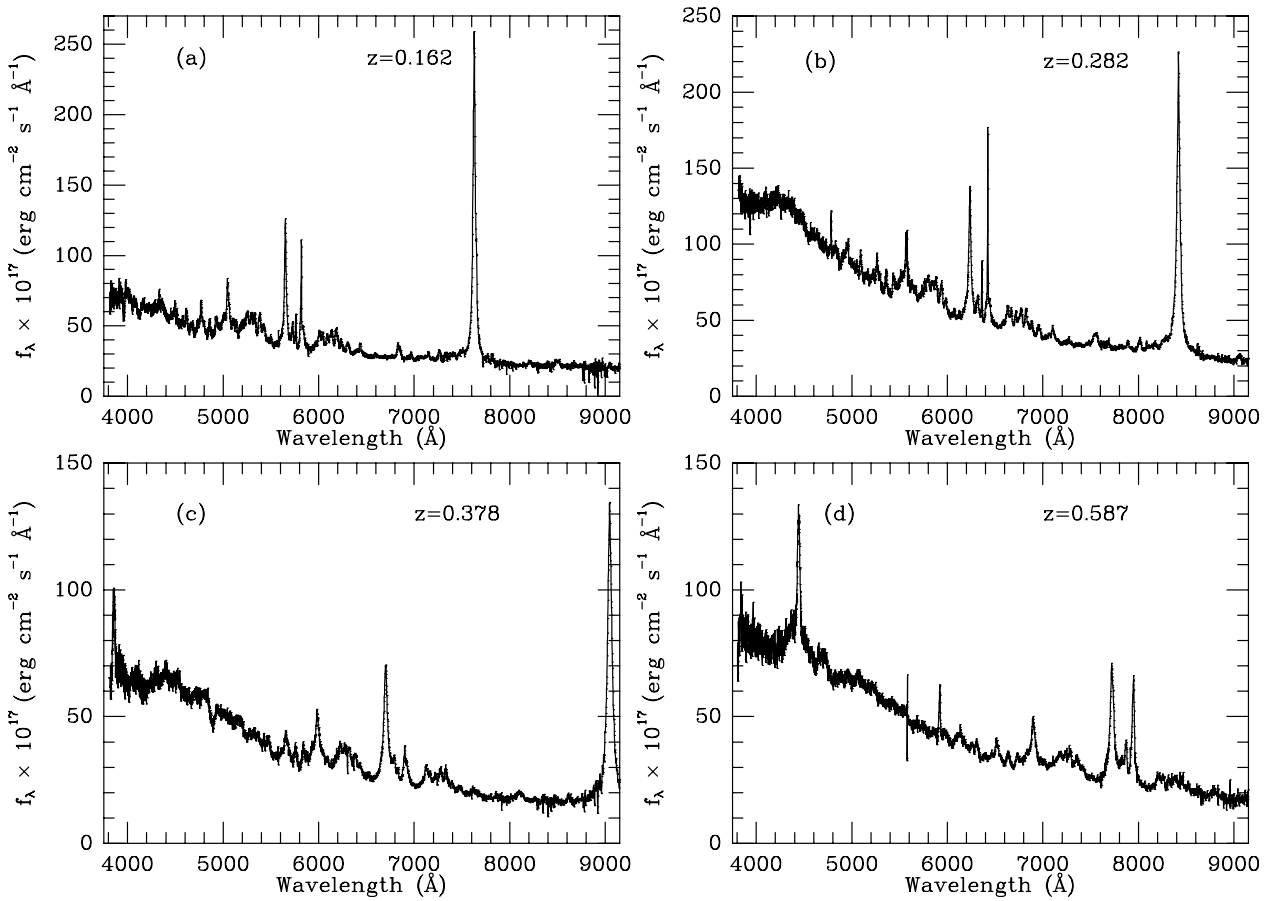

FIG. 5.—Example SDSS optical spectra for RASS/SDSS X-ray–emitting NLSy1's. There are 133 such confident NLSy1's (and another 36 possible ones) in this initial RASS/SDSS sample. (*a*) SDSS J090137.99+532051.1; (*b*) SDSS J125100.45+660326.7; (*c*) SDSS J024250.85−075914.3; (*d*) SDSS J134948.39−010621.8.

only permit accurate redshifts, but also quantitative classification (based on widths and line-ratios) into various AGN subclasses. In this section, we return to a discussion of the ensemble properties of our sample.

The optical magnitudes (Fig. 7*a*) for the quasars/AGNs extend over the entire range accessible to routine SDSS spectroscopy of $15 < m < 21$, though the median of $g = 18.7$ is typical of past related optical identification efforts. Interestingly, even at the brightest end, there are dozens of X-ray –emitting quasars/AGNs brighter than 17th magnitude that were not cataloged prior to SDSS. The redshift distribution for the quasars is also shown in Figure 7*b*, and again the median redshift of $z = 0.4$ is typical of previous identification work at similar X-ray flux levels. However, our initial RASS/SDSS AGN catalog already includes 23 suggested quasar counterparts at $z > 2$, including one possible identification even for a redshift $z = 3.56$ quasar.[22]

The distribution of offsets (Fig. 8) between the RASS X-ray positions and the SDSS optical positions is approximately as expected if the 1200 AGNs are indeed the proper identifications, at least in a statistical sense. For example, as shown in Figure 8*a*, 84% of the SDSS quasars/AGNs fall within 30″ of the RASS X-ray positions, in approximate agreement with independent expectations about the RASS positional uncertainty distribution as a function of X-ray detection likelihood (Voges et al. 1999); the latter may be derived from Tycho stars also detected in the RASS. Figure 8*b* shows a slightly different representation of these positional offset data, where now the offsets have been normalized relative to the RASS positional error; the latter accounts for the dependence of the RASS positional uncertainty on the X-ray source significance, total X-ray counts detected, etc. Figure 8*b* also confirms that the RASS positional error estimates are reasonable ones, e.g., with more than 97% of the suggested identifications found within an offset smaller than 3 times that predicted from the RASS X-ray positional error.

The small number with larger offsets (about 3% of the sample) is also consistent with the approximate expected number of random coincidences between SDSS quasars and the RASS error circles sampled, as we describe below.

We also show in Figure 9 one last related measure of the distribution of positional offsets between RASS X-ray sources and various extragalactic SDSS optical objects (having SDSS spectra). As one simple indicator of the association of various object subclasses with RASS X-ray sources, we display histograms of the distributions of the

[22] The $z = 4.9$ quasar SDSSp J173744.87+582829.5 mentioned in Anderson et al. (2001), which falls within (though rather far out in) a RASS error circle, is *not* confirmed as an X-ray source counterpart in the *Chandra* follow-up; the X-ray source has been positionally pinpointed in *Chandra* images by Vignali et al. (2003b) to fall well away (about 45″) from the high-redshift quasar.

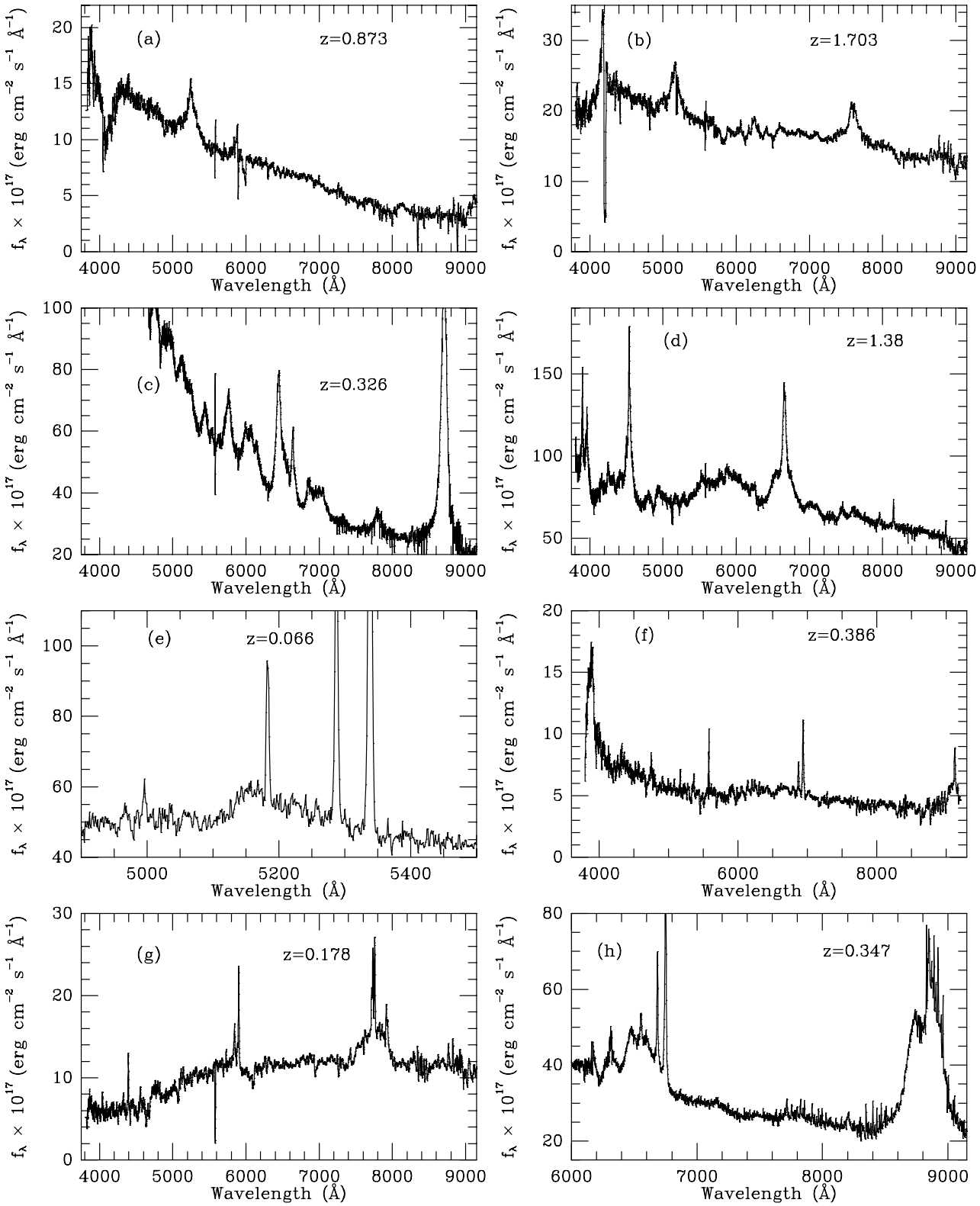

FIG. 6.—Selected other X-ray–emitting AGNs with unusual optical SDSS spectra. (*a*) SDSS J171216.28+660211.7 and (*b*) SDSS J150935.97+574300.5 are examples of *possible* X-ray–emitting quasars with BALs or mini-BALs, though certainly not yet confirmed definitively. (*c*) SDSS J134251.60−005345.2 and (*d*) SDSS J091301.01+525928.9 are examples of strong Fe quasars, with permitted line widths in excess of those usually associated with NLSy1's. (*e*) SDSS J172533.07+571645.5 is an example AGN with an asymmetric Hβ line profile. (*f*) SDSS J113615.08−002314.3 is an AGN with broad weak Hβ characteristic of Seyfert 1.8, but which has both strong and broad Hα and Mg II. (*g*) SDSS J155350.44+562230.8 is an example object with very wide line profiles on the order of 20,000 km s^{-1}. (*h*) SDSS J075407.95+431610.5 is an example of an X-ray–emitting AGN in the sample with highly unusual multiple-peaked emission line profiles.

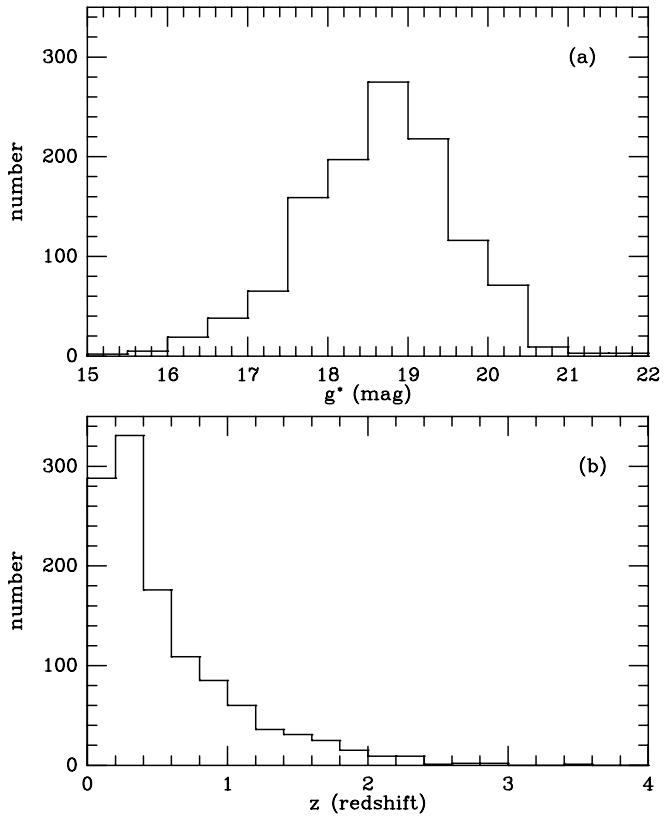

FIG. 7.—Distributions of (*a*) SDSS *g**-band magnitudes and (*b*) redshifts, for 1180 optical counterparts of RASS/SDSS X-ray–emitting AGNs (BL Lac candidates excluded here). Redshifts are obtained from the high-quality follow-up SDSS optical spectroscopy. The median magnitude and redshift are typical of similar identification surveys having comparable X-ray depths. However, the large sample size permits inclusion of a significant number of higher redshift objects as well.

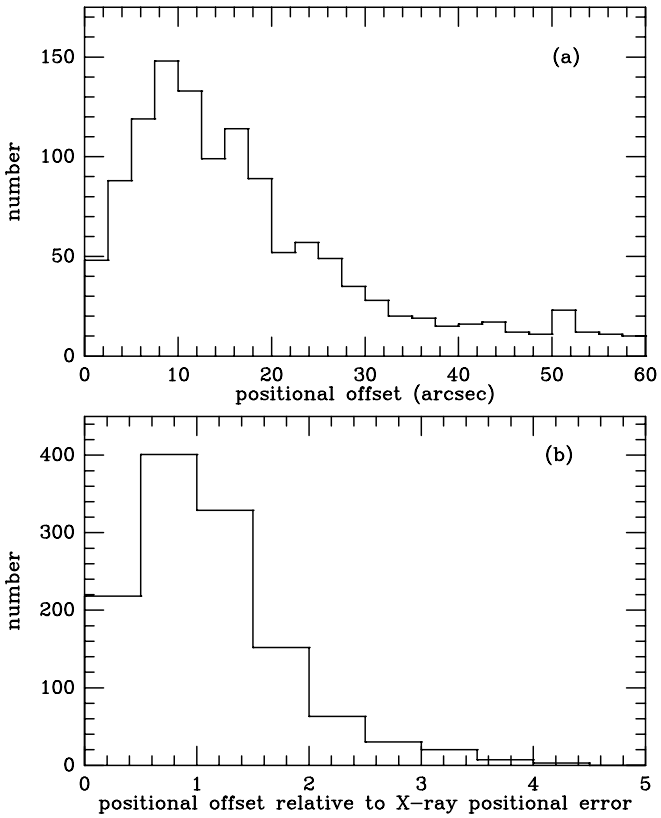

FIG. 8.—Distribution of positional differences between the SDSS optical positions of the 1225 quasar/AGN/BL Lac suggested identifications are approximately as expected if these are (statistically) the proper identifications. (*a*) The positional offsets in arcseconds are approximately as expected for the RASS positional accuracy, accounting for the range of X-ray detection likelihoods included. (*b*) The distribution of relative positional differences between the SDSS optical and RASS X-ray positions of the quasar/AGN/BL Lac identifications, in this case normalized to the expected RASS X-ray source positional error. (For ease of display, two objects with relative offsets >5 are excluded from this plot).

squares r^2 of the positional offsets between the SDSS optical positions and the RASS X-ray source positions; i.e., we count the fraction of objects falling within equal area annuli offset from the RASS X-ray source positions. For a chance superposition of SDSS objects within RASS error circles, these histograms would be approximately flat with r^2. We conservatively limit consideration (in Fig. 9) to objects that fall just within the $r < 27\farcs5$ offset discussed in § 3; all the "target selection" algorithms for selecting objects for SDSS fiber spectroscopy may work within this smaller region, while for greater offsets the "ROSAT" algorithms may not select targets for SDSS spectra (and therefore could produce an artificial truncation in the distributions for larger r^2). Figure 9 shows separate r^2 histograms for quasars/AGNs with predominant broad-lines (Fig. 9, *top left*) discussed in § 4.1, quasars/AGNs with narrower permitted lines (Fig. 9, *top right*) discussed in § 4.2, as well as the BL Lac candidates (Fig. 9, *bottom left*) discussed in § 4.3; in each of these cases, the histograms for the AGNs are very strongly peaked at small r^2 values, as expected if these AGNs are statistically the proper (i.e., with low contamination) X-ray source identifications.

For comparison, the lower right panel of Figure 9 shows the r^2 histogram for other normal galaxies (with weak or no emission) within $27\farcs5$ of RASS sources. (We have excluded error circles in which we have already identified the probable X-ray counterpart as among the 1225 AGNs discussed in §§ 4.1–4.3, or there is a previously known X-ray–emitting cluster). Although this figure suggests the possibility of a very weak statistical correlation between some of these galaxies and RASS X-ray sources, it especially confirms that contamination by random superpositions is very high for these normal galaxy cases—contamination an order of magnitude higher than for the AGNs/quasars. Although the ensemble of such more normal galaxies may well be suitable for follow-on "X-ray image stacking" or "survival analysis" statistical studies appropriate for samples with a large fraction of X-ray nondetections, they are not considered further in the current paper in which the focus is on secure X-ray source identifications of AGNs.[23]

A related estimate of the expected number of random coincidences of quasars/AGNs with RASS X-ray sources

[23] For example, one might consider looking for hidden AGNs among some brighter subset of such normal galaxies that also have small X-ray/optical positional offsets. Indeed, limiting consideration to $g < 18$ and offsets of less than $27\farcs5$ yields an r^2 distribution for 16 bright normal galaxies that is only a little less peaked than that seen for the AGNs in Fig. 9. However, these 16 galaxies are sufficiently bright in the optical that only two have $\log(f_x/f_{opt}) > 0.1$ and therefore significantly exceed the f_x/f_{opt} range observed for other normal galaxies (e.g., Stocke et al. 1991). The exceptions are a well-studied Virgo galaxy (NGC 4636) with an extended X-ray halo (e.g., Jones et al. 2002) and a radio galaxy RX J1725.3+5255 (e.g., Bade et al. 1998a) that may also be in a group or cluster.

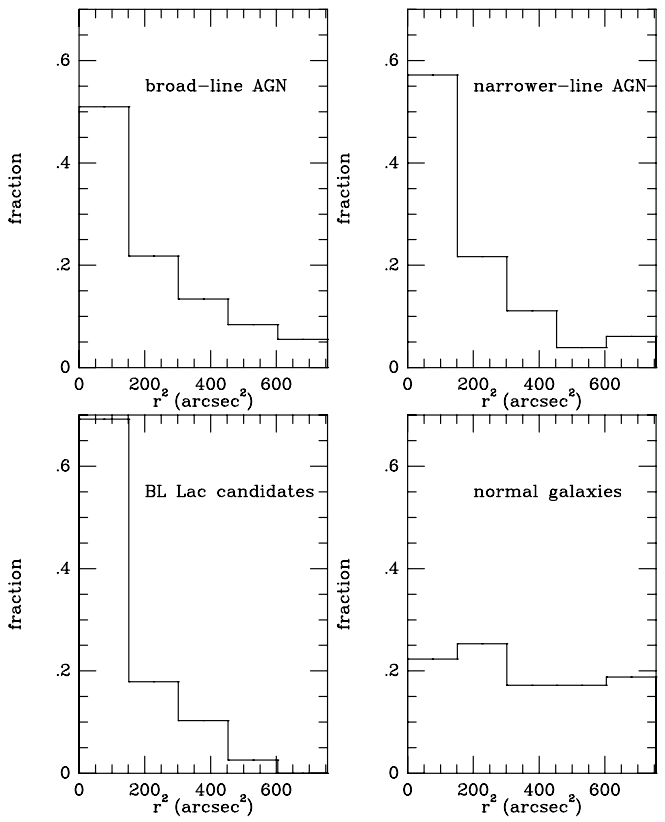

FIG. 9.—Another measure of the distribution of positional offsets between RASS X-ray sources and various extragalactic SDSS optical objects (having SDSS spectra). Plotted are histograms of the distributions of the squares r^2 of the positional offsets between the SDSS optical positions and the RASS X-ray source positions; we count the fraction of objects falling within equal area annuli offset from the RASS X-ray source positions. (We conservatively limit consideration to objects within $r < 27''.5$, where all relevant algorithms for SDSS spectroscopy may select targets, as discussed in § 6). Separate r^2 histograms are shown for quasars/AGNs with predominant broad lines (*top left*) discussed in § 4.1, quasars/AGNs with narrower permitted lines (*top right*) discussed in § 4.2, as well as BL Lac candidates (*bottom left*) discussed in § 4.3; in each of these cases, the histograms for the AGNs are very strongly peaked at small r^2 values, as expected if these AGNs are statistically the proper (i.e., with low contamination) X-ray source identifications. For comparison, the bottom right panel shows the histogram for normal SDSS galaxies (which, as anticipated, shows at most only a very weak statistical correlation with RASS X-ray sources).

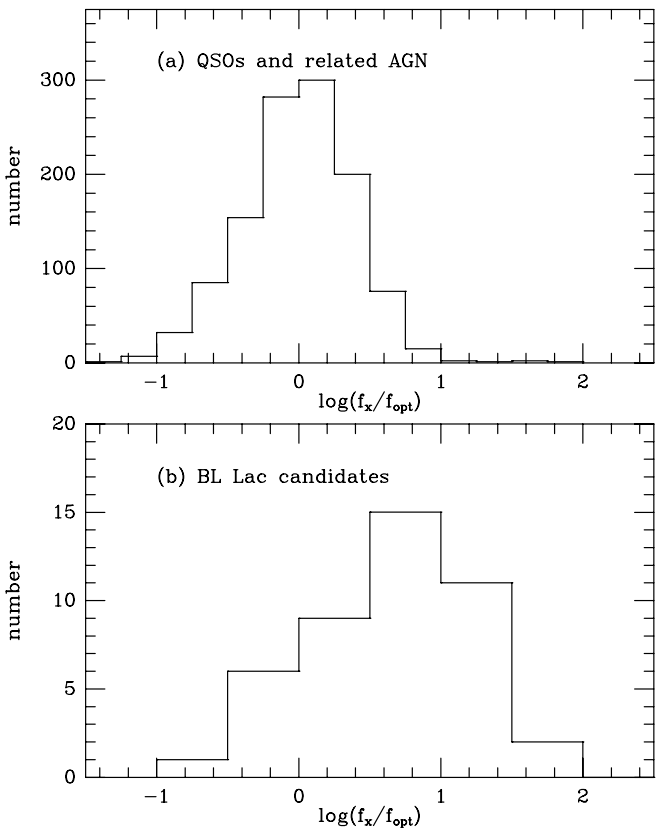

FIG. 10.—(*a*) The distribution of f_x/f_{opt} for the 1158 suggested quasar/AGN identifications having observed broad emission line regions (Seyfert 2 candidates are excluded) discussed in §§ 4.1 and 4.2. As expected if these are the proper identifications, typical quasars/AGNs are found to emit approximately as much energy in the X-ray as in the optical band. (*b*) The distribution of f_x/f_{opt} for the RASS/SDSS BL Lac candidate identifications discussed in § 4.3. The distribution is similar to that found in other X-ray selected BL Lac surveys (though markedly different than that of the emission-line quasars/AGNs shown in Fig. 9*a*).

further quantifies the statistical reliability of the cataloged quasar/AGN identifications. The surface density of SDSS *optically* selected quasars is on the order of 15 deg^2, while the combined area covered by all RASS error circles considered in the 1400 deg^2 area of this initial sample is less than about 4 deg^2. Thus, as the above positional arguments also suggest, only a small fraction (<5%) of the 1225 proposed quasar/AGN counterparts are likely to be spurious random chance positional coincidences, for which the RASS X-ray source and SDSS quasar/AGNs are in fact unrelated.

The distribution of the ratios of X-ray–to–optical flux for 1158 quasar/AGN identifications with observed broad emission line regions (we exclude the Seyfert 2 and BL Lac candidates, as both classes are known to have distinct flux ratios vs. broad-line AGNs) is also as expected for typical X-ray–emitting quasars/AGNs. It has been long recognized that roughly as much energy is emitted in the X-ray as in the optical bands, as is reaffirmed by the empirical distribution (Fig. 10*a*) of f_x/f_{opt} for the AGNs considered here. In estimating the flux ratio f_x/f_{opt}, we adopt for f_x the (corrected) 0.1-2.4 keV X-ray flux (from Tables 2 and 4) and estimate the optical broadband flux in a 4000–9000 Å bandpass using the *g*-band PSF magnitudes (again from Tables 2 and 4) and assuming an optical power law in energy with index $\alpha_o = 0.5$. The observed distribution (Fig. 10*a*) of f_x/f_{opt} for RASS/SDSS quasars/AGNs is very similar to that found for the EMSS quasars/AGNs (see Stocke et al. 1991).

Similarly, Figure 10*b* shows the distribution of f_x/f_{opt} ratios for the 45 RASS/SDSS BL Lac candidates discussed in § 4.3. Although distinctly different than the distribution for the quasars/AGNs in Figure 10*a*, the BL Lac distribution we find here is very similar to that found in earlier X-ray selected BL Lac samples (e.g., again see Stocke et al. 1991). The agreement of these f_x/f_{opt} distributions with expectations for both quasar/AGN and BL Lac classes, again further confirms that the great majority of the suggested RASS/SDSS AGN identifications are in fact likely correct.

7. DISCUSSION OF AN EXAMPLE MULTIWAVEBAND CORRELATION

The large survey sample size and uniformity and quality of observational data present a variety of opportunities for follow-on detailed studies of correlations between optical

and X-ray wavebands for AGNs. Although this paper presents primarily the initial catalog information, we also include here one illustrative example of the sample's potential use in studies of correlations between X-ray and optical wavebands.

As depicted in Figure 11, the 1158 X-ray–emitting AGNs with broad-line regions discussed in §§ 4.1 and 4.2 (Seyfert 2 and BL Lac candidates are again excluded for reasons discussed above) also appear to show the very long-recognized nonlinear correlation between optical and X-ray wavebands found in many earlier studies/samples (e.g., Avni & Tananbaum 1985). Although ours is, of course, an X-ray selected sample, the relationship we find (Figure 11*a*) between X-ray and optical monochromatic luminosity, $l_x \propto l_{opt}^{0.89\pm0.01}$, is in excellent agreement with (though with smaller formal errors than) that found in some optically selected samples also studied via *ROSAT* (e.g., see Green et al. 1995; Vignali et al. 2003a). This correlation is virtually unchanged when excluding the 12% of sample objects that are radio detected. However, the relation does appear to change when separately considering lower versus higher optical-luminosity objects; if we divide the sample in two at the median value $\log(l_{opt}) = 29.63$, we find $l_x \propto l_{opt}^{0.82\pm0.03}$ for the half of the objects above the median l_{opt}, and $l_x \propto l_{opt}^{0.98\pm0.03}$ for the half below the median (see also the discussion in the last paragraph of this section).

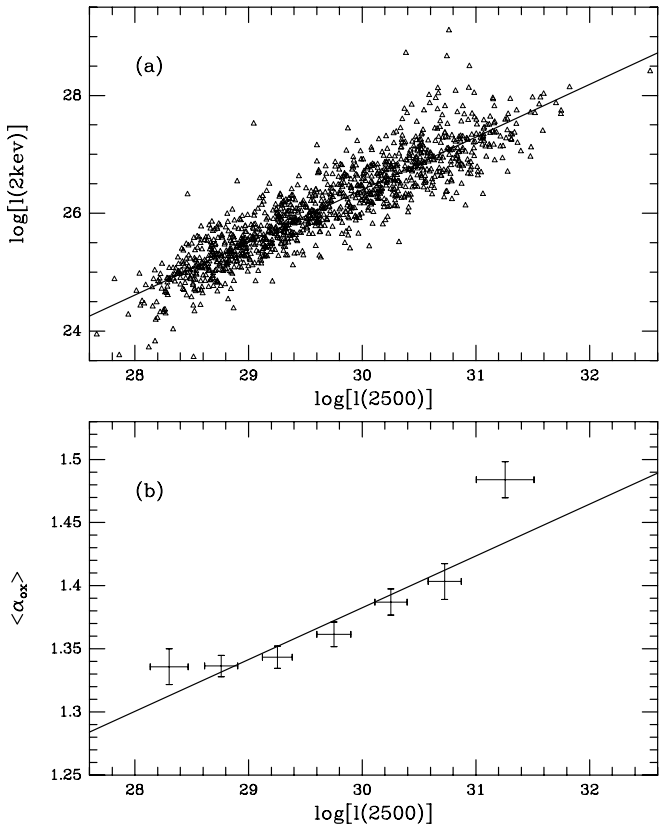

FIG. 11.—The long-recognized nonlinear relationship between X-ray and optical wavebands (logarithms of monochromatic luminosities in cgs units at 2 keV and 2500 Å are shown) is also seen here in our large X-ray selected sample of 1158 quasars/AGNs (with broad emission line regions; Seyfert 2 and BL Lac candidates are excluded). (*a*) The solid line is a least-squares fit to the $l_{2\,keV}$ vs. l_{2500} data, with slope 0.89 ± 0.01. (*b*) Similar consistent results are obtained when alternately regressing α_{ox} against optical luminosity, and in this case linear regression yields $\alpha_{ox} \propto l_{opt}^{0.041\pm0.005}$, equivalent as expected to $l_x \propto l_{opt}^{0.89}$. The solid line is the best-fit regression relation (fitted to all 1158 points), while the error bars show the mean and the standard error in the mean value of $\langle\alpha_{ox}\rangle$, as well as the mean and standard deviations in optical luminosity, when considering averages taken in various optical luminosity bins (typically with 70–220 points per bin). There is an indication of a possibly more complex relation than assumed in the simple regression model.

Similar consistent results are obtained when alternately regressing α_{ox} against optical luminosity. For the same total ensemble of 1158 quasars/AGNs with observed broad-line regions, this regression yields $\alpha_{ox} \propto l_{opt}^{0.041\pm0.005}$, equivalent as expected to $l_x \propto l_{opt}^{0.89}$. Figure 11*b* depicts this latter relationship in a slightly different form. The solid line is the best-fit regression relation (fitted to all 1158 points), while the error bars show the mean and the standard error in the mean value of α_{ox}, as well as the mean and standard deviations in optical luminosity, when considering averages taken in various optical luminosity bins. (Note that the vertical error bars reflect the very large number of data points [typically 70–220] averaged together to estimate $\langle\alpha_{ox}\rangle$ in each bin.)

Figure 11*b* once again suggests the possibility of more complex dependences than assumed in our simple regression of α_{ox} versus $\log(l_{opt})$ [or in the equivalent $\log(l_x)$ versus $\log(l_{opt})$ relation discussed above]. Moreover, the general sense of little dependence of α_{ox} on l_{opt} at lower values of l_{opt}, but a stronger dependence at higher l_{opt} values has also been suggested by some other studies (e.g., Yuan et al. 1998a). We caution however, that a detailed study would necessarily include a proper account of selection biases, dispersions in the quantities used in the regression, multiple possible parameter dependencies (e.g., on redshift and radio luminosity), and other aspects that we have neglected here. For example, disparate dispersions in optical compared with X-ray luminosities can yield apparent, but spurious, nonunity slopes in such simple correlation analyses between l_{opt} and l_x (e.g., Yuan, Siebert, & Brinkmann 1998b). Nonetheless, this illustrative example suggests that the large size, uniformity and quality of optical and X-ray data, and range of physical parameters covered by the RASS/SDSS sample are well-suited to a variety of more detailed follow-on multiwaveband correlation studies.

8. SUMMARY

The SDSS optical and RASS X-ray surveys are well-matched to each other via a variety of fortunate circumstances, allowing efficient large-scale identification of X-ray source optical counterparts. SDSS and RASS imaging catalog data are autonomously cross-correlated, and software algorithms are employed to automatically select, and assign priorities to, candidate optical counterparts for follow-on SDSS fiber spectroscopy. Application of this approach to initial SDSS data has provided homogeneous identification and RASS/SDSS flux and spectroscopic data for a large sample of X-ray–emitting quasars and other kinds of AGNs. The combination of SDSS multicolor selection and RASS data—and in some cases FIRST radio information—is highly (>75%) efficient for selection of X-ray–emitting quasars/AGNs. In an initial 1400 deg^2 of sky considered, more than 1200 plausible X-ray–emitting quasars/AGNs have been optically identified, including numerous rare cases such as 45 BL Lac candidates and more than 130 NLSy1's. As this initial area represents only a fraction of the ultimate joint RASS/SDSS sky coverage, $\sim 10^4$ fully

and homogeneously characterized X-ray source counterpart identifications may be anticipated to follow by completion of the SDSS survey. The already large sample will allow for a variety of more detailed studies of various AGN subclasses and individual objects of special interest, as well as for studies of ensemble correlations between optical and X-ray wavebands.

Funding for the creation and distribution of the SDSS Archive[24] has been provided by the Alfred P. Sloan Foundation, the Participating Institutions, the National Aeronautics and Space Administration, the National Science Foundation, the US Department of Energy, the Japanese Monbukagakusho, and the Max Planck Society. The SDSS is managed by the Astrophysical Research Consortium (ARC) for the Participating Institutions. The Participating Institutions are the University of Chicago, Fermilab, the Institute for Advanced Study, the Japan Participation Group, the Johns Hopkins University, Los Alamos National Laboratory, the Max Planck Institute for Astronomy (MPIA), the Max Planck Institute for Astrophysics (MPA), New Mexico State University, the University of Pittsburgh, Princeton University, the US Naval Observatory, and the University of Washington.

The authors thank the late Donald Baldwin of the University of Washington for his tireless contributions to the success of SDSS.

[24] For the SDSS Web site see http://www.sdss.org.

REFERENCES

Abazajian, K., et al. 2003, AJ, 126, 2081
Anderson, S. F., et al. 2001, AJ, 122, 503
Avni, Y., & Tananbaum, H. 1986, ApJ, 305, 83
Avni, Y., Worrall, D. M., & Morgan, W. A. 1995, ApJ, 454, 673
Bade, N., et al. 1998a, A&AS, 127, 145
———. 1998b, A&A, 334, 459
Baldwin, J. A., Phillips, M. M., & Terlevich, R. 1981, PASP, 93, 5
Becker, R. H., White, R. L., & Helfand, D. J. 1995, ApJ, 450, 559
Blanton, M. R., Lupton, R. H., Maley, F. M., Young, N., Zehavi, I., & Loveday, J. 2003, AJ, 125, 2276
Boller, T. 2000, NewA Rev., 44, 387
Boyle, B. J., McMahon, R. G., Wilkes, B. J., & Elvis, M. 1995, MNRAS, 272, 462
Collinge, M. J., et al. 2003, in preparation
Condon, J. J., et al. 1998, AJ, 115, 1693
Dressler, A., & Schectman, S. 1987, AJ, 94, 899
Fischer, J.-U., Hasinger, G., Schwope, A. D., Brunner, H., Boller, T., Trümper, J., Voges, W., & Neizvestny, S., 1998, Astron. Natchr., 319, 347
Fukugita, M., Ichikawa, T., Gunn, J. E., Doi, M., Shimasaku, K., & Schneider, D. P. 1996, AJ, 111, 1748
Gallagher, S. C., et al. 1999, ApJ, 519, 549
Gallo, L., et al. 2003, in preparation
Giacconi, R., Gursky, H., Paolini, F., & Rossi, B. 1962, Phys. Rev. Lett., 9, 439
Gioia, I. M., Maccacaro, T., Schild, R. E., Stocke, J. T., Liebert, J. W., Danziger, I. J., Kunth, D., & Lub, J. 1984, ApJ, 283, 495
Green, P. J., Aldcroft, T. L., Mathur, S., Wilkes, B. J., & Elvis, M. 2001, ApJ, 558, 109
Green, P. J., et al. 1995, ApJ, 450, 51
Gunn, J. E., et al. 1998, AJ, 116, 3040
Halpern, J. P., Turner, T. J., & George, I. M. 1999, MNRAS, 307, L47
Hogg, D. W., Schlegel, D. J., Finkbeiner, D. P., & Gunn, J. E. 2001, AJ, 122, 2129
Jones, C., Forman, W., Vikhlinin, A., Markevitch, M., David, L., Warmflash, A., Murray, S., & Nulsen, P. E. J. 2002, ApJ, 567, L115
Kauffmann, G., et al. 2003, MNRAS, 341, 33
Kewley, L. J., Dopita, M. A., Sutherland, R. S., Heisler, C. A., & Trevena, J. 2001, ApJ, 556, 121
Laurent-Muehleisen, S. A., Kollgaard, R. I., Ryan, P. J., Feigelson, E. D., Brinkmann, W., & Siebert, J. 1997, A&AS, 122, 235
Lupton, R. H., Gunn, J. E., & Szalay, A. 1999, AJ, 118, 1406
Margon, B., Chanan, G. A., & Downes, R. A. 1982, ApJ, 253, L7
Margon, B., et al. 2000, BAAS, 32, 1183
McHardy, I. M., et al. 1998, MNRAS, 295, 641
Morris, S. L., Stocke, J. T., Gioia, I., Schild, R. E., Wolter, A., Maccacaro, T., & della Ceca, R. 1991, ApJ, 380, 49
Newberg, H. J., & Yanny, B. 1997, ApJS, 113, 89
Perlman, E. S., et al. 1996, ApJS, 104, 251
Pfeffermann, E., Briel, U. G., Hippmann H., et al., 1987, Proc. SPIE, 733, 519
Pier, J. R., Munn, J. A., Hindsley, R. B., Hennessy, G. S., Kent, S. M., Lupton, R. H., & Ivezíc, Z. 2003, AJ, 125, 1559
Pogge, R. W. 2000, NewA Rev., 44, 381
Rector, T. A., Stocke, J. T., & Perlman, E. S. 1999, ApJ, 516, 145
Richards, G. T., et al. 2002, AJ, 123, 2945
Schartel, N., et al. 1996, MNRAS, 283, 1015
Schlegel, D. J., Finkbeiner, D. P., & Davis, M. 1998, ApJ, 500, 525
Schwope, A., et al. 2000, Astron. Nachr., 321, 1
Schneider, D. P., et al. 2002, AJ, 123, 567
Sheldon, E. S., et al. 2001, ApJ, 554, 881
Smith, J. A., et al. 2002, AJ, 123, 2121
Stark, A. A., Gammie, C. F., Wilson, R. W., Bally, J., Linke, R. A., Heiles, C., & Hurwitz, M. 1992, ApJS, 79, 77
Stocke, J. T., Morris, S. L., Gioia, I. M., Maccacaro, T., Schild, R., Wolter, A., Fleming, T. A., & Henry, J. P. 1991, ApJS, 76, 813
Stoughton, C., et al. 2002, AJ, 123, 485
Strateva, I., et al. 2003, AJ, 126, 1720
Szkody, P., et al. 2002, AJ, 123, 430
———. 2003, AJ, 126, 1499
Urry, C. M., & Padovani, P. 1995, PASP, 107, 803
Vignali, C., Brandt, W. N., & Schneider, D. P. 2003a, AJ, 125, 433
Vignali, C., et al. 2003b, AJ, 125, 2876
Voges, W., et al. 1999, A&A, 349, 389
———. 2000, IAU Circ. 6420
———. 2001, in Proc. IAU Colloq. 184, AGN Surveys, ed. R. F. Green, E. Ye. Khachikian, & D. B. Sanders (ASP Conf. Ser. 284) (San Francisco: ASP), 25
———. 2003, in preparation
Whittle, M. 1992, ApJS, 79, 49
Wilkes, B. J., Tananbaum, H., Worrall, D. M., Avni, Y., Oey, M. S., & Flanagan, J. 1994, ApJS, 92, 53
Williams, R.J., Pogge, R. W., & Mathur, S. 2002, AJ, 124, 3042
York, D. G., et al. 2000, AJ, 120, 1579
Yuan, W., Brinkmann, W., Siebert, J., & Voges, W. 1998a, A&A, 330, 108
Yuan, W., Sibert, J., & Brinkmann, W. 1998b, A&A, 334, 498
Zakamska, N. L., et al., AJ, 2003, 126, 2125
Zickgraf, F.-J., Engels, D., Hagen, H.-J., Reimers, D., & Voges, W. 2003, A&A, 406, 535
Zickgraf, F.-J., Krautter, J., Appenzeller, I., Thiering, I., Voges, W., Mujica, R., Pakull, M. W., Serrano, A., & Chavarria, C. 1998, Astron. Nachr., 319, 42